



HAL
open science

Implementation and impacts of surface and blowing snow sources of Arctic bromine activation within WRF-Chem 4.1.1

Louis Marelle, Jennie L. Thomas, Shaddy Ahmed, Katie Tuite, Jochen Stutz, Aurélien Dommergue, William R. Simpson, Markus M. Frey, Foteini Baladima

► To cite this version:

Louis Marelle, Jennie L. Thomas, Shaddy Ahmed, Katie Tuite, Jochen Stutz, et al.. Implementation and impacts of surface and blowing snow sources of Arctic bromine activation within WRF-Chem 4.1.1. *Journal of Advances in Modeling Earth Systems*, 2021, 13 (8), pp.e2020MS002391. 10.1029/2020ms002391 . insu-03266425v1

HAL Id: insu-03266425

<https://insu.hal.science/insu-03266425v1>

Submitted on 21 Jun 2021 (v1), last revised 15 Aug 2021 (v2)

HAL is a multi-disciplinary open access archive for the deposit and dissemination of scientific research documents, whether they are published or not. The documents may come from teaching and research institutions in France or abroad, or from public or private research centers.

L'archive ouverte pluridisciplinaire **HAL**, est destinée au dépôt et à la diffusion de documents scientifiques de niveau recherche, publiés ou non, émanant des établissements d'enseignement et de recherche français ou étrangers, des laboratoires publics ou privés.



Distributed under a Creative Commons Attribution - NoDerivatives 4.0 International License

Implementation and impacts of surface and blowing snow sources of Arctic bromine activation within WRF-Chem 4.1.1

Louis Marelle^{1,2}, Jennie L. Thomas^{1,2}, Shaddy Ahmed¹, Katie Tuite³, Jochen Stutz³, Aurlien Dommergue¹, William R. Simpson⁴, Markus M. Frey⁵, Foteini Baladima¹

¹Universit de Grenoble Alpes, CNRS, IRD, IGE, Grenoble, France

²LATMOS/IPSL, Sorbonne Universit, UVSQ, CNRS, Paris, France

³Department of Atmospheric and Oceanic Sciences, University of California, Los Angeles, CA, USA

⁴Geophysical Institute and Department of Chemistry and Biochemistry, University of Alaska Fairbanks, Fairbanks, AK, USA

⁵British Antarctic Survey, Natural Environment Research Council, Cambridge, UK

Key Points:

- Halogen activation and its role in Arctic surface ozone depletion events (ODEs) is modeled using WRF-Chem.
- Two halogen activation mechanisms are implemented (1) surface snow and (2) blowing snow.
- A spring 2012 case study indicates that both mechanisms can trigger near-surface ODEs, but that surface snow dominates.

Corresponding author: Louis Marelle, louis.marelle@latmos.ipsl.fr

Corresponding author: Jennie Thomas, jennie.thomas@univ-grenoble-alpes.fr

This article has been accepted for publication and undergone full peer review but has not been through the copyediting, typesetting, pagination and proofreading process, which may lead to differences between this version and the [Version of Record](#). Please cite this article as [doi: 10.1029/2020MS002391](https://doi.org/10.1029/2020MS002391).

This article is protected by copyright. All rights reserved.

Abstract

Elevated concentrations of atmospheric bromine are known to cause ozone depletion in the Arctic, which is most frequently observed during springtime. We implement a detailed description of bromine and chlorine chemistry within the WRF-Chem 4.1.1 model, and two different descriptions of Arctic bromine activation: (1) heterogeneous chemistry on surface snow on sea ice, triggered by ozone deposition to snow (Toyota et al., 2011), and (2) heterogeneous reactions on sea salt aerosols emitted through the sublimation of lofted blowing snow (Yang et al., 2008). In both mechanisms, bromine activation is sustained by heterogeneous reactions on aerosols and surface snow. Simulations for spring 2012 covering the entire Arctic reproduce frequent and widespread ozone depletion events, and comparisons with observations of ozone show that these developments significantly improve model predictions during the Arctic spring. Simulations show that ozone depletion events can be initiated by both surface snow on sea ice, or by aerosols that originate from blowing snow. On a regional scale, in spring 2012, snow on sea ice dominates halogen activation and ozone depletion at the surface. During this period, blowing snow is a major source of Arctic sea salt aerosols but only triggers a few depletion events.

Plain Language Summary

During Arctic spring, ground level ozone is often depleted to very low concentrations compared to background levels. This surface ozone depletion is caused by reactive halogen species in the atmosphere, especially bromine. In this study, we implement a detailed description of chlorine and bromine chemistry in the regional atmospheric model WRF-Chem 4.1.1. We also compare two different bromine sources capable of triggering these events: first, chemical reactions on surface snow over sea ice, and second, sea salt particles emitted by the sublimation of salty “blowing snow” lofted by strong winds. These developments are used to investigate the origins of Arctic bromine and of ozone depletion events, and to improve the representation of Arctic ozone in the model. We find that, in spring 2012, both bromine sources can cause ozone depletion events, but that over the entire Arctic, snow on sea ice dominates halogen activation and causes ground level ozone depletion.

1 Introduction

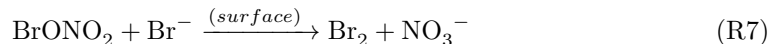
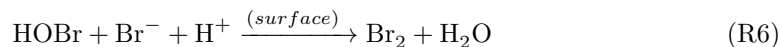
During Arctic spring, the Atmospheric Boundary Layer (ABL), experiences episodic depletion of ozone to values less than 10 parts per billion by volume (ppbv), far below background levels of ~ 40 ppbv (Oltmans, 1981; Barrie et al., 1988). These well-known ozone depletion events (ODEs) are tied to the presence of enhanced concentrations of reactive bromine in the atmosphere (Barrie et al., 1988), including species such as Br_2 , BrO , Br , HOBr , and BrNO_3 (Platt & Hönninger, 2003; Simpson et al., 2007b; Abbatt et al., 2012; Pratt et al., 2013; Simpson et al., 2015). Although the link between increased bromine in the atmosphere and ozone depletion events was discovered over three decades ago (Barrie, 1986), developing predictive model descriptions of bromine emissions and chemistry in polar regions remains a challenge (Yang et al., 2008; Toyota et al., 2011; Falk & Sinnhuber, 2018; Fernandez et al., 2019; Huang et al., 2020; Herrmann et al., 2021). At present, most models used to predict Arctic scale or global ozone largely ignore or only include simplified descriptions of these processes and do not correctly predict boundary layer ozone concentrations during the Arctic spring (see for example Monks et al., 2015; Emmons et al., 2015). Since ozone is a key atmospheric oxidant and plays a role in virtually all other atmospheric oxidant cycles (e.g. $\text{HO}_x = \text{OH} + \text{HO}_2$) and acts as a greenhouse gas, inaccurate predictions of Arctic ozone severely limit our ability to understand past and future polar atmospheric chemistry. In addition, the key link between ozone, halogens, and sea ice/snow cover is essential in order to predict future polar conditions and interpret past ice core records and sea ice conditions (Spolaor et al., 2013, 2016).

70 Finally, atmospheric bromine also cause mercury oxidation in the Arctic boundary layer,
 71 leading to atmospheric mercury depletion events (AMDEs) and deposition to the cryosphere
 72 and ecosystems. Better predicting Arctic mercury oxidation, and human exposure there-
 73 fore also requires more realistic representation of Arctic halogen chemistry.

74 The key emitted species that triggers bromine explosion events, ODEs and AMDEs
 75 is molecular bromine (Br_2), which is photolysed (R1) to form bromine atoms (Br) that
 76 quickly react with ozone (R2). This forms another key gas phase species in the reactive
 77 bromine/ozone cycle, bromine monoxide (BrO), which can react with HO_2 to form HOBr
 78 (R3). HOBr then photolyzes (R4) to form OH and Br, which has two main impacts. First,
 79 the Br radical goes on to further propagate the ozone destruction cycle. Second, the net
 80 effect of both (R3) and (R4) is that one HO_2 radical is converted to the more reactive
 81 OH radical. This can increase the amount of OH relative to HO_2 present during bromine
 82 activation, potentially increasing the oxidation rate of chemical species (e.g. volatile or-
 83 ganic gases) within the ABL. BrO also undergoes self reaction to reform Br_2 (R5), which
 84 is the dominant Br_2 formation pathway under sufficiently high BrO concentrations. The
 85 resulting effect of equations R1 to R5 is rapid ozone loss, causing ODEs.



91
 92
 93
 94
 95 The source of atmospheric bromine in the Arctic is undoubtedly bromide (Br^-) that
 96 is present in trace amounts in the ocean, and is activated via heterogeneous reactions
 97 on surfaces (snow, aerosols, etc). Recycling of reactive bromine via gas phase and het-
 98 erogeneous reactions on surfaces is crucial in sustaining significant concentrations of at-
 99 mospheric bromine that cause ODEs. Without this recycling, the quantity of reactive
 100 bromine (present in pptv levels) in the atmosphere is too small to sufficiently deplete ozone
 101 (present in ppbv levels). Recycling of bromine on surfaces can occur via reactions involv-
 102 ing HOBr (R6) and BrONO_2 (R7) on salty surfaces, resulting in re-release of Br_2 to the
 103 atmosphere. These heterogeneous processes are what make bromine species incredibly
 104 active during polar spring and capable of depleting ozone to near-zero values. Reactive
 105 bromine cycling is terminated when reactive bromine is deactivated upon formation of
 106 species that do not undergo gas phase photochemistry or that are inefficient at reform-
 107 ing reactive bromine via heterogeneous reactions (e.g. HBr).



110
 111 While numerous theories have been discussed as to how bromine is released to the
 112 atmosphere, two main mechanisms, both relying on salty snow, have been tested in 3D
 113 numerical models. The first mechanism has proposed that activation of bromine occurs
 114 via reactions on surface snow present on sea ice, followed by further recycling of bromine
 115 on land and sea ice based snowpacks (Toyota et al., 2011). It also involves heterogeneous
 116 recycling on aerosols present within the atmosphere to sustain halogen activation. This
 117 mechanism has been tested in the 3D models GEM-AQ and EMAC (Toyota et al., 2011,
 118 2014; Falk & Sinnhuber, 2018), and very recently WRF-Chem (Herrmann et al., 2021).
 119 There is experimental evidence for this surface snow mechanism: Pratt et al. (2013) re-
 120 ported the photo-chemical production of molecular bromine from surface snow using chem-
 121 ical ionization mass spectroscopy (CIMS) based on Arctic snow chamber experiments.

122 It has also been shown that bromine activation correlates with the occurrence of first-
123 year sea ice (Simpson et al., 2007a; Bougoudis et al., 2020), and that it can also occur
124 over snow found on multi-year sea ice (Peterson et al., 2019). These surfaces are sim-
125 ilar in that both first year and multi year ice are usually snow covered.

126 The second mechanism that has been proposed is that bromine activation occurs
127 on aerosols originating from sublimation of salty blowing snow. Under high wind con-
128 ditions, snow is lofted into the atmosphere and undergoes sublimation to form new sea
129 salt particles in the atmosphere. Fresh sea salt aerosols (primarily sodium chloride, NaCl)
130 contain trace amounts of bromide that undergo heterogeneous chemistry to release re-
131 active bromine to the atmosphere (Yang et al., 2008, 2010; Huang & Jaeglé, 2017; Yang
132 et al., 2019), which is fastest in the presence of sunlight (i.e. photo-chemical reactions
133 are occurring). There is recent direct evidence for the role of blowing snow in forming
134 sea salt aerosols in the Antarctic (M. Frey et al., 2020). Model studies on polar aerosols
135 also demonstrate an improved agreement compared to sea salt observations for winter
136 and spring when blowing snow sourced sea salt aerosols are included (Rhodes et al., 2017;
137 Huang et al., 2018). Further, this has been recently shown to improve model predictions
138 of BrO and O₃ (Huang et al., 2020; Yang et al., 2020). Finally, observations show that
139 aerosols can sustain bromine activation above the boundary layer (Peterson et al., 2017),
140 but it has not yet been clearly demonstrated from measurements that blowing snow sourced
141 sea salt aerosols trigger bromine explosion events.

142 Bromine chemistry is influenced by numerous polar processes including: light avail-
143 ability (influenced by cloud cover, latitude, and season), atmospheric boundary layer dy-
144 namics, mixing between the free troposphere and ABL, occurrence of high winds/storms,
145 and other factors (e.g. stratospheric influences). There is a delicate interplay between
146 atmospheric dynamics, emissions, recycling and chemistry, which determines when bromine
147 activation results in significant observable impacts on atmospheric chemistry (Jones et
148 al., 2009; Peterson et al., 2015). For example, the very stable atmospheric boundary lay-
149 ers often found over ice/snow correspond to slow vertical mixing/dispersion and low wind
150 speeds (e.g. Anderson & Neff, 2008). These conditions likely favor the importance of sur-
151 face emissions from snow on sea ice by concentrating these emissions into a small vol-
152 ume, allowing for the bromine explosion cycle to take off (e.g. Swanson et al., 2020). Con-
153 versely, high wind conditions that are found during storms favor blowing snow and blow-
154 ing snow sourced aerosol formation. Blowing snow sourced aerosols are also likely to be
155 most important when the ocean is mostly ice covered, suppressing open ocean sea salt
156 aerosol production (Huang et al., 2018). High winds also indicate that the ABL is not
157 clearly separated from the free troposphere, allowing air masses containing high bromine
158 to be lofted from the surface to higher altitudes where they can be more easily detected
159 above clouds via satellite remote sensing (Blechschmidt et al., 2016). These complex fac-
160 tors, must be taken into account when considering Arctic halogen chemistry within dif-
161 ferent 3D modeling frameworks and model evaluations using observations. In this study,
162 we focus on very near surface processes and model evaluation using near surface obser-
163 vations within the ABL.

164 In this work, we implement a bromine and chlorine chemistry mechanism in an ad-
165 vanced regional meteorological model that includes atmospheric chemistry, the Weather
166 Research and Forecasting coupled with Chemistry (WRF-Chem) model, to study spring-
167 time ODEs in the Arctic in 2012. We include, for the first time two different halogen ac-
168 tivation and recycling mechanisms and we study their individual contributions to Arc-
169 tic ozone depletion events for one example season, spring 2012. Section 2 describes the
170 model setup and an optimized meteorological setup to simulate Arctic boundary layer
171 dynamics and mixing. Section 3 describes the new model developments implemented in
172 WRF-Chem 4.1.1. In section 4, we evaluate the performance of these developments by
173 comparing model results with surface measurements of ozone and BrO taken at multi-
174 ple Arctic sites. In section 5 we use these new developments to investigate what triggers

175 Arctic ozone depletion events, and to better understand their impacts on Arctic atmo-
176 spheric chemistry. We put our results and spring 2012 into the long term meteorolog-
177 ical and ozone depletion context in section 6. Finally, the lessons learned are discussed
178 in section 7.

179 2 Methodology

180 2.1 WRF-Chem model setup

181 In order to reproduce observed ozone depletion events in the Arctic, we add bromine
182 and chlorine chemistry in the WRF-Chem 4.1.1 model (Grell et al., 2005; Fast et al., 2006).
183 We perform these developments in a version of WRF-Chem already optimized for Arc-
184 tic aerosols and ozone (Marelle et al., 2017), but that to date did not include a descrip-
185 tion of halogen chemistry. New developments are integrated to the SAPRC-99 gas-phase
186 chemistry scheme (Carter, 2000), coupled with MOSAIC-8bin sectional aerosol scheme
187 (Zaveri et al., 2008) within WRF-Chem 4.1.1, due to its skill at reproducing boundary
188 layer aerosols and ozone (outside of ozone depletion events). MOSAIC includes secondary
189 organic aerosols (SOA), aqueous chemistry, and already includes chlorine aerosol species
190 including heterogeneous ClNO₂ formation from N₂O₅.

191 Photolysis rates are calculated by the Fast-J scheme (Wild et al., 2000). Cloud mi-
192 crophysics are represented by the Morrison 2-moment scheme (Morrison et al., 2009),
193 and cumuli by the KF-CuP scheme (Berg et al., 2015), which are both coupled to MO-
194 SAIC aerosols (wet removal, cloud chemistry, tracer transport, aerosol activation). Long-
195 wave and shortwave radiation calculations are performed in the RRTMG scheme (Iacono
196 et al., 2008). Initial and boundary conditions for aerosols and trace gases are from the
197 Model for Ozone and Related chemical Tracers, version 4 (MOZART-4, Emmons et al.,
198 2010). We chose a model domain centered over the Arctic (domain shown in Figure 1)
199 with a horizontal resolution of 100 km × 100 km to encompass the entire Arctic with
200 a vertical resolution of 72 levels up to a pressure of 50 hPa. All simulations are performed
201 between the dates 1 March 2012 and 31 April 2012. The first 7 days are model spin up
202 and are excluded from the analysis.

203 2.2 Optimized meteorological setup for accurate boundary layer dynam- 204 ics

205 An accurate representation of boundary layer dynamics, especially boundary layer
206 stability, is particularly critical for vertical mixing and non-linear atmospheric chemistry
207 within the ABL. For this reason, we tested and evaluated multiple WRF dynamics con-
208 figurations in order to select the meteorological options and the global model driving ini-
209 tial and boundary conditions. We tested 2 different global meteorological datasets ERA-
210 Interim (Dee et al., 2011) and NCEP FNL (Final Analysis, National Centers for En-
211 vironmental Prediction, 2000). We also tested 3 different land surface models: the Noah
212 Land Surface Model (NoahLSM, Tewari et al., 2004), the Noah land surface model with
213 MultiParameterization options (NoahMP, Niu et al., 2011), and the Community Land
214 Model version 4 (CLM4, Oleson et al., 2010). In addition, we tested three different bound-
215 ary layer schemes: the Yonsei University Scheme (YSU, Hong et al., 2006), the MellorYa-
216 madaJanjic Scheme (MYJ, Janji, 1994), and the MellorYamada Nakanishi Niino Level
217 2.5 Scheme (MYNN2, Nakanishi & Niino, 2009).

218 Because not all combinations of options were compatible with each other and with
219 the chemistry and aerosol schemes, in total 13 simulations were completed (Table 1). Sim-
220 ulated 2-meter temperatures from these 13 runs are compared to observations at Utqiagvik,
221 Alaska (NOAA/ESRL/GMD Baseline Observatories, <https://www.esrl.noaa.gov/gmd/dv/data/>).
222 In addition, modeled vertical temperature profiles at Utqiagvik, Alaska are compared
223 to measurements from the Integrated Global Radiosonde Archive (IGRA, Durre et al.,

224 2006), provided twice a day at 11 UTC and 23 UTC. The model is evaluated using ra-
225 diosondes below 500 meters (altitude above ground level), to evaluate the structure of
226 the lowest portion of the troposphere where halogen chemistry is active. Table 1 shows
227 the root-mean-square errors (RMSEs) and correlations between each chosen setup and
228 these two observational datasets.

229 Since boundary layer structure is critical in capturing dispersion and chemistry of
230 surface emissions, we chose the setup with the highest correlation with IGRA radiosonde
231 measurements. This good agreement is illustrated in Figure 2. This setup uses the FNL
232 (final) analysis from NCEP for initial conditions, boundary conditions and spectral nud-
233 ging; the Noah Land Surface Model; and the MYNN2 boundary layer scheme with the
234 MYNN2 surface layer. This setup also performs well against other metrics. Figure 2 also
235 illustrates that even though it does not have the best agreement with 2-meter temper-
236 atures at Utqiagvik, the model performance there is still very good. The following model
237 runs are therefore all performed with this model setup.

238 3 New model developments in WRF-Chem 4.1.1

239 We have added to the model chlorine and bromine gas phase reactions including
240 photolysis (section 3.1), heterogeneous halogen reactions on aerosols (section 3.2), dry
241 and wet deposition of halogen species (section 3.3), and emissions of bromine from sea-
242 ice, snow, and open oceans (section 3.4). The version of the model used in this study and
243 the input files are publicly available as Marelle et al. (2021).

244 3.1 Gas-phase chlorine and bromine chemistry

245 We add 82 additional gas-phase chemical reactions involving chlorine and bromine,
246 and 50 additional gas-phase species, to the Kinetic PreProcessor (KPP) within WRF-
247 Chem. These reactions are taken from a combination of prior modeling work on chlo-
248 rine and bromine chemistry (Gratz et al., 2015; von Glasow et al., 2002a, 2002b; Piot
249 & Glasow, 2009; Thomas et al., 2011, 2012a).

250 These 82 new gas-phase reactions include 15 photolysis reactions. The new pho-
251 tolysis rates are calculated in the Fast-J photolysis scheme in WRF-Chem (Wild et al.,
252 2000), using absorption cross sections and quantum yields from IUPAC (Atkinson et al.,
253 2008, ; <http://iupac.pole-ether.fr/>). Cross-sections and yields are taken from NASA JPL
254 instead (Burkholder et al., 2015) when species were not found in IUPAC (BrO, OClO),
255 or when JPL data were more spectrally resolved or covered a larger spectral range (Br₂,
256 BrNO₂). In order to be used in Fast-J, the JPL and IUPAC cross sections at high spec-
257 tral resolution are weighted by the solar spectrum and distributed to the 7 coarse Fast-
258 J spectral bins. The preprocessor used to perform this interpolation (Wild et al., 2000)
259 is available along with input files at <https://github.com/lmarelle/FastJ-preprocessor>

260 3.2 Heterogeneous reactions involving halogens

261 Heterogeneous reactions on aerosols containing bromine or chlorine are an impor-
262 tant step sustaining activation of gaseous halogen species in the Arctic. We include a pa-
263 rameterized representation of halogen heterogeneous chemistry in the SAPRC-99 MOSAIC-
264 8bin scheme within WRF-Chem, for the 12 heterogeneous reactions presented in Table 2.
265 Following Dentener and Crutzen (1993), we assume that the rate limiting factor in these
266 heterogeneous reactions is the uptake of gaseous species on the aerosol. The heteroge-
267 neous reactive uptake coefficient γ is corrected by the unitless factor, J , which is depen-
268 dant on γ and the Knudsen number (Kn). J_n represents the limitation of reaction at
269 the aerosol surface due to gas diffusion limitations, which is calculated for each aerosol
270 size bin following equation 1 in Fuchs and Sutugin (1971), as presented in Seinfeld and
271 Pandis (1998).

$$J_n = \frac{0.75\gamma(1 + Kn)}{Kn^2 + Kn + 0.283Kn \times \gamma + 0.75\gamma} \quad (1)$$

We model the heterogeneous reaction rate k (s^{-1}) following equation (2) as a product of J , the total aerosol area density A (cm^{-1}), the mean molecular speed (\bar{v} , given in cm s^{-1}), γ , and the yield (ϕ) representing the weight of the different possible reaction pathways for a given species on the aerosol (such that the sum of the different reaction yields for a given species is 1). The γ values for each reaction and yields used are given in Table 2. Reaction rates are calculated for each of the eight MOSAIC aerosol size bins and then summed to obtain the heterogeneous reaction rate.

$$k = \sum_{i=1}^{n=8} 0.25\phi\bar{v}\gamma A_i J_i \quad (2)$$

This approach allows us to represent the effect of heterogeneous chemistry on the gas phase, without explicitly calculating the full chemistry in the aerosol phase. In order to limit the computational cost of the new scheme, we do not model aerosol bromine explicitly either, since adding an additional aerosol species in the MOSAIC-8bin aerosol scheme adds 16 advected tracers to the scheme (8 interstitial aerosol bins and 8 cloud-borne). In order to lighten the mechanism and still maintain mass conservation for bromine, reactions consuming aerosol-phase bromine (e.g. $\text{HOCl} \xrightarrow{\text{(aerosol)}} \text{BrCl}$) are rewritten using HBr as a proxy for aerosol bromine (e.g. $\text{HOCl} + \text{HBr} \rightarrow \text{BrCl}$) (Table 2). For each of these reactions, the heterogeneous reaction rate is divided by the HBr concentration in KPP, to keep the kinetics independent of the HBr concentration while still consuming HBr (following Badia et al., 2019)

For consistency and to simplify model developments, we use the same approach, using HCl, for heterogeneous reactions consuming chlorine in aerosols, even though chlorine aerosols are represented explicitly in MOSAIC-8bin. The only exception is the heterogeneous formation of ClNO_2 through N_2O_5 , which is already calculated explicitly in MOSAIC in WRF-Chem 4.1.1.

Some of these heterogeneous reactions might require acidic conditions to proceed (Abbatt et al., 2012). For aerosols that have a pH calculated in MOSAIC, we chose an aerosol pH threshold of 5, above which the heterogeneous reaction rates (equation 1) are set to 0. This pH condition is checked for each aerosol size bin independently, before calculating the summed reaction rates for the full aerosol population in equation 2.

3.3 Dry and wet deposition of halogen species

We include dry deposition for 7 new halogen species: Br_2 , HOBr , HBr , BrONO_2 , Cl_2 , HOCl and ClONO_2 . Dry deposition is neglected for all other new species. Dry deposition is calculated through the resistance scheme of Wesely (1989). This scheme requires 4 parameters for each new species: the effective Henry's law constant (H^*); the Henry's law temperature correction factor (DHR); the deposition reactivity parameter (f_0 , representing the reactivity of the species when in contact with the ground surface); and the molecular diffusivity of the species (dv_j). The values of these variables for the 7 new species are presented in Table 3. H^* and DHR are taken from Sander (2015), f_0 from Toyota et al. (2011), and dv_j is taken as the inverse square root of the species molecular weight, in g mol^{-1} .

Wet removal of HCl was already included in WRF-Chem 4.1.1. We added to the model wet deposition of HBr , HOBr , BrONO_2 , HOCl and ClONO_2 by impaction scavenging, using a first-order scavenging rate constant of $3.89 \times 10^{-4} \text{ s}^{-1}$ per mm h^{-1} of precipitation (Toyota et al., 2011).

317

3.4 Emissions of bromine from sea-ice, snow, and open oceans

318

319

320

321

Emissions of bromine in the Arctic have been attributed to multiple sources including sea-ice (first-year and multi-year), snow surfaces, sea salt from blowing snow, and oceanic sea salt. We implemented descriptions of these emission sources in WRF-Chem 4.1.1, which are described in the following sections.

322

3.4.1 Br_2 emissions from surface snow

323

324

325

326

327

328

329

Surface snow bromine activation follows Toyota et al. (2011). In this mechanism, deposition of atmospheric oxidants to the snowpack over sea ice releases Br_2 to the atmosphere, and this process is photochemically accelerated in the presence of sunlight. In practice, the Br_2 emission flux is calculated as proportional to the O_3 dry deposition flux, with a proportionality factor depending on solar zenith angle. In sunlit conditions (solar zenith angle $\leq 85^\circ$), Br_2 emissions are 0.075 times the deposition flux, and in dark conditions, 0.001 times.

330

3.4.2 Br_2 emissions from blowing snow

331

332

333

334

335

336

The blowing snow parameterization is based on Yang et al. (2008) and Huang and Jaeglé (2017). Blowing snow events start when the 10-m wind speed, w_{10} , is above the threshold $w_{10_{crit}}$, which is a function of surface temperature (Yang et al., 2008). Lofted snow sublimates in the atmosphere depending on environmental conditions, releasing sea salt aerosols and Br_2 . In WRF-Chem 4.1.1, we calculate the Br_2 emission flux, E_{Br_2} ($kg\ m^{-2}\ s^{-1}$), following equation 3.

337

$$E_{Br_2} = \sum_{i=1}^{n=8} E_{NaCl}(bin) \times R_a \times DF \quad (3)$$

338

339

340

341

342

343

344

345

346

347

348

Where $E_{NaCl}(bin)$ is the sea salt emission flux from blowing snow in a given MOSAIC aerosol size bin ($kg\ m^{-2}\ s^{-1}$), R_a is the mass ratio between bromine and NaCl in sea water (0.00233), and DF is the maximum bromine depletion factor of 0.38 from Yang et al. (2008), based on Sander et al. (2003), representing the fraction of aerosol bromine lost to the atmosphere. This maximum value for the depletion factor represents an estimate of bromine emissions emitted during the whole atmospheric lifetime of the blowing-snow sourced sea salt aerosols. This constant value was chosen to limit the computational cost of the new scheme, since in reality bromine emissions from sea salt aerosols depend on heterogeneous chemistry on the aerosols, which can only be resolved by explicitly tracking the simulated size-resolved aerosol bromine chemistry and resulting aerosol bromide content.

349

350

The sea salt emissions in each MOSAIC aerosol size bin, $E_{NaCl}(bin)$, are calculated following equation 4.

351

$$E_{NaCl}(bin) = \frac{q_s \xi}{1000} \int_{D_{low}(bin)}^{D_{high}(bin)} f(D_{dry}) dD_{dry} \quad (4)$$

352

353

354

355

356

357

358

Where q_s is the snow sublimation flux ($kg\ m^{-2}\ s^{-1}$), calculated as a function of local wind speed, temperature and humidity (Yang et al., 2008). In equation 4, $D_{high}(bin)$ and $D_{low}(bin)$ are also the lower and upper dry diameter range of a given MOSAIC aerosol size bin, $f(D_{dry})$ is the snow size distribution expressed as a function of dry sea salt aerosol size (Yang et al., 2008), and ξ is a uniform snow salinity of 0.1 psu (Huang & Jaeglé, 2017). Following Huang and Jaeglé (2017), we also assume that each snow flake emits $N = 5$ sea salt aerosols.

359

360

361

Available values of salinity from the Antarctic differ by more than an order of magnitude (Rhodes et al., 2017). The Massom et al. (2001) distribution used in Yang et al. (2008) has a mean value of 8.3 psu, 83 times higher than the Arctic value used in our

362 implementation. No pan-Arctic measurements of snow and snow on sea ice salinity cur-
 363 rently exist, but recent measurements in the central Arctic (M. M. Frey & Nomura, 2019)
 364 found snow salinities with a median value of 0.02 psu and a mean of 1.7 psu. Here, we
 365 use the parameters from Huang and Jaeglé (2017) ($\xi = 0.1$ psu, $N = 5$), which are in
 366 the middle of this range, and were shown to improve model agreement with observed sea
 367 salt aerosol concentrations at Utqiagvik. In agreement with Huang and Jaeglé (2017),
 368 we show (Supplementary Figure S1) that the chosen values for ξ and N produce more
 369 realistic sea salt aerosol concentrations at Arctic coastal sites than the original Massom
 370 et al. (2001) salinity and $N = 1$ value used in Yang et al. (2008). We also show that
 371 low salinity values of 0.01 psu match observations even better than 0.1 psu, while a rea-
 372 sonable high bound of 1.7 psu leads to overestimations of Na aerosols by up to 2 orders
 373 of magnitude.

374 *3.4.3 Bromine recycling on surface snow*

375 Br_2 emitted to the atmosphere by either surface snow or blowing snow can be trans-
 376 formed into HOBr and BrONO_2 . When deposited on sea ice and snow, these species can
 377 be recycled back into atmospheric Br_2 by surface reactions in the snowpack. Following
 378 Toyota et al. (2011), we assume that all HOBr and BrONO_2 deposited on sea ice is re-
 379 emitted as Br_2 . This assumes an unlimited supply of Br^- in snow over sea ice. Unlike
 380 Toyota et al. (2011), we assume that this recycling is independent of sea ice age, since
 381 recent observations indicate that multiyear ice can be an efficient source of Br_2 (Peterson
 382 et al., 2019). Over continental snow, Br^- availability in the snowpack is assumed to be
 383 limited by HBr deposition. As a result, the Br_2 emission rate there is limited by the HBr
 384 deposition rate, and is taken as the smaller flux between HBr and HOBr+ BrONO_2 .

385 *3.4.4 Temperature and ice fraction dependence of bromine emissions 386 and recycling*

387 Recent observations indicate that Br_2 emissions and recycling can occur at tem-
 388 peratures up to 0°C (Burd et al., 2017). For this reason, we removed the temperature
 389 threshold of -15°C used in Toyota et al. (2011) for surface emissions, and replaced it by
 390 a 0°C threshold that applies for all Br_2 emission processes over surface snow (surface snow,
 391 blowing snow, surface recycling). When the skin temperature over snow or ice exceeds
 392 the 0°C threshold in a grid cell (i.e. when snow starts to melt), the grid cell stops emit-
 393 ting bromine until the end of the simulation.

394 Snow on sea ice is also influenced by sea ice flooding events, which are more com-
 395 mon for thinner and lower fractional sea ice cover (Provost et al., 2017). These events
 396 may deactivate snow on sea ice by changing the pH and/or structure of the snow to less
 397 active for bromine release. Due to this, we include a cutoff for halogen activation and
 398 recycling on snow on sea ice that is dependent on the grid cell sea ice fraction. We test
 399 different fractional sea ice cutoff values (see electronic supplement), which are discussed
 400 further in section 4.

401 *3.4.5 Direct Br_2 emissions from open oceans*

402 Sea salt emitted from open oceans can also release bromine to the atmosphere. We
 403 include this source of atmospheric Br_2 in the model, following equation 5.

$$404 \quad E_{\text{Br}_2, \text{ocean}} = E_{\text{NaCl}, \text{ocean}} \times R_a \times DF \quad (5)$$

405 Where $E_{\text{NaCl}, \text{ocean}}$ is the sea salt emission flux from the ocean surface ($\text{kg m}^{-2} \text{ s}^{-1}$),
 406 already calculated in WRF-Chem 4.1.1 for ice-free ocean grid cells (Gong et al., 1997).
 407 We added emissions from open leads in sea ice in WRF-Chem 4.1.1 by calculating the
 408 flux for fractional sea ice cells, and scaling it by the open ocean fraction in the cell. R_a

409 is the same $Br/NaCl$ mass ratio already used in the blowing snow parameterization, and
410 DF is a mean depletion factor of 0.25.

411 4 Model results and evaluation

412 In order to evaluate the updated model, we performed 4 different WRF-Chem sim-
413 ulations, listed in Table 4, and compared them to surface ozone and BrO observations
414 at 5 different Arctic locations. First, we perform a reference simulation with no halogen
415 chemistry and no updates implemented (NOHALO), and one simulation (BOTH) includ-
416 ing all our halogen chemistry developments with both the surface activation mechanism
417 (section 3.4.1), and the blowing snow parameterization (section 3.4.2). In order to un-
418 derstand which initial source of atmospheric bromine, (1) surface snow or (2) blowing
419 snow, triggers ozone depletion events in the Arctic, we perform 2 additional simulations,
420 SURFACE and BLOWING. SURFACE is a simulation with only the surface mechanism
421 included, where blowing snow emissions are excluded. BLOWING is the simulation with
422 only the blowing snow source, where surface emissions presented in section 3.4.1 are ex-
423 cluded; however we note that the BLOWING simulation still includes bromine recycling
424 on the snow surface (section 3.4.3), even though it was not included in the original pub-
425 lications of Yang et al. (2008) and Huang and Jaeglé (2017). For the BOTH simulation,
426 we have tested four different fractional sea ice coverage cutoff values for both halogen
427 activation and recycling mechanisms to be active; 15%, 50%, 75%, and 90% (see Section 3.4.4).
428 Based on these tests (Figures S2 and S3 in the electronic supplement), we have chosen
429 a 75% fractional sea ice cover cutoff for all simulations presented.

430 4.1 Surface ozone and BrO evaluation at Utqiagvik, Alaska

431 The comparison between observed and modeled concentrations of O_3 and BrO at
432 Utqiagvik, AK (formerly Barrow, AK) is shown in Figure 3. Surface observations of ozone
433 in Utqiagvik are from NOAA-ESRL (<https://www.esrl.noaa.gov/gmd/dv/data/>). BrO
434 is measured by a ground-based (0-200 m) MAX-DOAS in Utqiagvik (BROMEX cam-
435 paign, described in Simpson et al. (2017)). WRF-Chem surface Br_2 concentrations (0-
436 200 m average) are also shown. Model results are spatially interpolated at the location
437 of the measurements, using only land grid cells.

438 The simulation including both mechanisms (BOTH), captures the observations more
439 accurately than the base version of the model (NOHALO). The RMSE of O_3 in BOTH
440 is 10 ppbv, compared to 25 ppbv in NOHALO (detailed statistics are given in supple-
441 mentary Table S1). The variability of ozone is also captured in the model when both emis-
442 sion mechanisms are implemented (correlation coefficient of 0.50 in BOTH, compared
443 to 0.22 in NOHALO). The amount and timing of ozone depletion events are generally
444 well represented, including both large scale ODEs that occur during the simulation pe-
445 riod as well as smaller ozone depletion/regeneration events. At this site, surface snow
446 activation (SURFACE simulation) is the main operating mechanism for ozone depletion
447 as it captures most of the large ODEs and smaller peak fluctuations (RMSE 10.3 ppbv,
448 correlation 0.50). The blowing snow mechanism (BLOWING simulation) does influence
449 the modeled ozone levels to a small extent for most of the simulation period, however,
450 it is only able to entirely capture the first ODE of the simulation (starting 8 March 2012)
451 indicating this particular event may be initiated by blowing snow. These developments
452 are able to significantly improve the representation of modeled ODEs, yet reproducing
453 the full nature of all events remains a challenge.

454 Similarly, Figure 3 shows that the timing of enhanced BrO concentrations repro-
455 duced by the model is comparable to the observational data during both periods of in-
456 creasing and declining BrO concentrations. However, from March 20th to March 30th mod-
457 eled BrO is underestimated, and from April 8th to April 11th it is overestimated; this
458 may be due to several factors. It is not likely to be caused by measurement error, since

459 Simpson et al. (2017) found that during March 2012, the typical error in BrO measure-
460 ment was 2 to 3 pptv. However, the same study found that BrO retrievals were highly
461 correlated at a 30 km scale only as long as sea ice was unbroken. At 100 km resolutions
462 and at a later period in April when leads are more likely to open, it is possible that the
463 WRF-Chem grid cell averages are less representative of measurements at Utqiagvik. In
464 addition, bromine activation and recycling is sensitive to boundary layer stability, and
465 even recent reanalysis datasets or advanced regional models such as WRF still struggle
466 to reproduce stable boundary layers over snow (C. Wang et al., 2019; Sterk et al., 2015).

467 Figure 3 also shows that extended periods of very low O₃ concentrations are some-
468 times associated with low concentrations of BrO. Under these conditions of low ozone
469 concentrations, BrO formation is limited by the fact that there is no ozone for Br atoms
470 to react with. In this case, other unobserved species, such as BrNO_y compounds, may
471 play a role in sustaining bromine chemistry by regenerating Br₂ (S. Wang et al., 2019).
472 Similar to ozone depletion, the surface snow mechanism plays the most important role
473 in determining enhanced BrO concentrations as well as high modeled Br₂ mixing ratios
474 at Utqiagvik, AK.

475 **4.2 Surface ozone evaluation at 4 additional Arctic stations and 2 Arc-** 476 **tic Ocean buoys**

477 In addition to improvements at Utqiagvik, we also report improvements in model
478 representation of ozone and ODEs at other Arctic locations. Figure 4 compares the sim-
479 ulated ozone to observations at: Station Nord, Greenland; Tiksi, Russia; Summit, Green-
480 land; Zeppelin Station, Svalbard, and at 2-Arctic buoys in the central Arctic (latitude
481 > 85N), O-buoy4 and O-buoy6 (Simpson et al., 2009; Knepp et al., 2010; Halfacre et al.,
482 2014). Table S1 also gives metrics (RMSE and correlation) at these sites. For high-altitude
483 sites (Summit and Zeppelin), model O₃ was interpolated at the altitude of the measure-
484 ments, even though this altitude was not located in the lowest model level. At all sites
485 except buoys, spatial interpolation is performed using only land grid cells. Figure 4 (and
486 supplementary Table S1) shows that when the surface scheme or both mechanisms are
487 included, modeled ozone concentrations are greatly improved in Nord, Greenland; Tiksi,
488 Russia, and at buoys in the Central Arctic.

489 At Station Nord (Figure 4a), a coastal site in the north of Greenland, the base run
490 with no halogen chemistry misses main features of the observed spring ozone mixing ra-
491 tios in 2012, including ODEs. The BLOWING model simulation has little influence on
492 ozone. We note that we have not tuned the parameters of the surface or blowing snow
493 bromine production mechanism to match observations, so it is possible that this and other
494 events will be better captured upon adjusting the parameters to our model. As imple-
495 mented, the surface snow mechanism (SURFACE) captures the timing and features of
496 most events (RMSE = 12.9 ppbv, R=0.33, compared to 17.2 ppbv and 0.17 for NOHALO).
497 At Station Nord, including both mechanisms (BOTH) does not significantly improve the
498 model compared to the surface snow mechanism alone (RMSE = 12.4 ppbv, R=0.34),
499 indicating that blowing snow has limited influence on modeled ozone at this station.

500 For Tiksi (Figure 4b), a coastal site in Russia, only the surface snow mechanism
501 reproduces the magnitude of observed ODEs. A long ozone depletion event occurs be-
502 tween 9 and 16 March. For this event, the SURFACE simulation predict earlier ozone
503 recovery to background levels. A second ODE, observed in between 22 March and 1 April,
504 is captured by both the SURFACE and BOTH runs, but only very weak ozone deple-
505 tion occurs in the BLOWING model run. Later, following April 15th, the decay of ozone
506 for an extended period of time is captured by the SURFACE snow model run, but not
507 by the BLOWING simulation. This suggests that in this season, the main operating mech-
508 anism is surface snow.

509 At Summit (Figure 4c, a high altitude non-coastal Arctic site) ozone depletion con-
510 ditions are not observed. This is due to the high altitude of the site, influenced by free
511 troposphere air masses, and the distance between Summit and the Arctic Ocean. Ob-
512 servations of halogen chemistry at Summit have been completed during other seasons
513 and found 2-3 pptv of bromine can be present during late spring/early summer (Stutz
514 et al., 2011; Liao et al., 2011), however these concentrations are not thought to cause ODEs.
515 In our runs, we have some active bromine chemistry at Summit that arrives via surface
516 snow and aerosol recycling from activation of oceanic bromine sources (Thomas et al.,
517 2012b). However, the influence of this chemistry is overestimated in our model descrip-
518 tion and should be investigated further in the future. When using a higher sea ice cover
519 threshold for halogen chemistry of 90% (Supplementary Figure S3), results from BOTH
520 and SURFACE are improved at Summit. Using this higher cutoff disables bromine emis-
521 sions near Southern Greenland, indicating that some incomplete or missing process in
522 our model (ice flooding, bromine depletion in snow, snow ageing or melt) should disable
523 bromine emissions from these areas. These discrepancies do not persist later in the model
524 run, after April 12th.

525 At the Zeppelin observatory (Figure 4d, near coastal mountain site) there is no clear
526 signature from blowing snow in modeled ozone depletion. Some of the model-observation
527 discrepancies for the SURFACE simulation can be explained by the coarse horizontal res-
528 olution of 100 km, which is not able to resolve the topography and the local mountain
529 meteorology. Despite these limitations, surface snow does predict the first low ozone event
530 (20 ppbv prior to March 15th), even though the mechanism results in too much ozone
531 depletion. The model then captures a series of ozone depletion events following April 1st,
532 but the BOTH and SURFACE runs remain depleted in ozone while the observations show
533 that ozone recovers quickly. During this period the NOHALO and BLOWING simula-
534 tion better reproduces the observation. The model cannot be evaluated for several days
535 due to a period of missing measurements centered around April 15th. Then, the model
536 does capture the amount, but not the timing of an ozone depletion event at the end of
537 April. The final event is captured by the SURFACE run.

538 Observations at very high latitudes at O-buoy4 and O-buoy6 indicate that ozone
539 is very often completely depleted in the Central Arctic in Spring 2012. Only the SUR-
540 FACE simulation (and BOTH) are able to reproduce this very low ozone, although BLOW-
541 ING reproduces partial depletion around 15-25 March at O-buoy4, and between 16-18
542 April at O-buoy6. Average observed ozone at O-buoy4 during the whole period is 6.7 ppbv
543 (vs. 8.6 ppbv in SURFACE). O-buoy6 only has limited data coverage (15 days in late
544 April), and experienced data quality issues (baseline levels are at -1.1 ppbv, corrected
545 on Figure 4f by assuming that the error is a constant offset), but it measured average
546 ozone of 1.3 ppbv during this limited period, also consistent with the 2.0 ppbv average
547 in SURFACE.

548 In summary, the timing and intensity of the ODEs in the BOTH and SURFACE
549 simulation best captures the overall features within the observations, although the in-
550 tensities of some events can be either over or underestimated. The average RMSE and
551 correlation of SURFACE against ozone at the 7 locations shown in Figures 4 and 3 is
552 10.2 ppbv and 0.37 respectively, compared to 19.4 ppbv and 0.28 for BLOWING (sup-
553plementary Table S1). In addition, we show on supplementary Figure S10 that this is
554 not likely to be due to our choice of parameters for the blowing snow scheme: lower and
555 upper bound snow salinities of 0.01 psu and 1.7 psu still do not reproduce observations
556 as well as SURFACE. The blowing snow simulation with 1.7 psu reproduces observed
557 ozone at Zeppelin relatively well, however supplementary Figure S1 shows that it also
558 produces far too much sea salt at the same site, indicating that bromine emissions by
559 blowing snow are overestimated by the scheme at Zeppelin. In almost all cases, surface
560 snow activation can then be seen as the dominant mechanism for ozone depletion in March-
561 April 2012.

5 Origins and impacts of springtime Arctic ozone depletion

5.1 Origin of ozone depleted air masses at Utqiagvik

To identify the origin of ozone-rich and ozone-depleted air masses, we use the Lagrangian particle dispersion model FLEXPART-WRF (Brioude et al., 2013), which is a version of the FLEXPART model (Stohl et al., 2005) driven by the WRF meteorological model. Using the meteorological fields from the WRF-Chem simulation described in section 2.1, we use FLEXPART-WRF in backward mode to study the source and transport of ozone-rich (measured $O_3 > 30$ ppb) and ozone-depleted (measured $O_3 < 10$ ppb) air masses during the month of April 2012. For each case, a fixed number of air parcels were released every hour when observed ozone was above or below these thresholds, so that the total number of parcels released from Utqiagvik, AK was 100,000. For the ozone-rich air, this represented a total of 68 releases during the month of April, and for the ozone-depleted air this included 388 releases. Each simulation was run backwards in time for 7 days to track the origin of air measured at Utqiagvik, AK and to study source-receptor relationships. To do this, we use surface potential emission sensitivities (PES), calculated by FLEXPART-WRF, which indicates when air was in contact with the surface and would be sensitive to emissions. PES values are given as the amount of time spent by parcels in each grid cell during the simulation.

Figure 5a shows the 0-100 m (surface) PES column, which represents the area where ozone-depleted air (< 10 ppbv) originates from. These air masses originate predominantly from over sea ice for the entire 7 day period prior to measurement. Figure 5b shows the 0-5000 m PES (consistent with the air altitude in Figure 5c), which shows that high ozone air (> 30 ppbv) is subject to long range transport across the Arctic from Siberia during the 7 days prior to arriving at Utqiagvik. Figure 5c shows the mean altitude of the transported plumes for low and high ozone air. This shows that during periods of high ozone, the air descends down from the free troposphere prior to measurement at the surface. This downward vertical mixing of ozone rich air from the free troposphere is important for replenishing ozone, and may also allow for new initiation of bromine activation on surface snow. It also allows for generation of BrO in the boundary layer for conditions where bromine is present but BrO is not formed due to complete ozone depletion. This shows there is a complex interplay between triggering at the surface and replenishment of ozone from above the boundary layer, mixed down from aloft. Conversely, during low ozone periods air remains near the surface, where it is more sensitive to surface and blowing snow emissions and to chemistry occurring on sea salt aerosols within the boundary layer (Figure 5).

5.2 Impacts on Pan-Arctic surface O_3 , BrO, and HO_x during spring 2012

The independent roles of the two halogen activation mechanisms on surface ozone and BrO concentrations, as well as their effect on Br_2 emissions, are illustrated in Figure 6. Here, we plot results for the SURFACE (left panels: a, d, g), BLOWING (center panels: b, e, h), and BOTH (right panels: c, f, i) runs, compared to the NOHALO base case, to illustrate how each mechanism activates bromine and impacts ozone.

We plot the total Br_2 emissions increase from each mechanism in Figures 6a-c. The most active Br_2 emissions from surface snow are located on the coastal Arctic. Due to the lack of multi-year sea ice in 2012 and the recent evidence that bromine is activated from snow on multi-year sea ice (Peterson et al., 2019), we do not distinguish ice type in the surface snow activation mechanism. This is evident in the emissions from snow on sea ice, which occurs for all sea-ice covered regions. The key trigger for initial Br_2 emissions is ozone deposition to sea ice in the surface snow mechanism, therefore emissions may be limited by the lack of ozone deposition when ozone has been depleted to near zero levels in the center of the Arctic (Figure 6g, discussed below, and supplementary Figure S6). For the blowing snow mechanism, the Br_2 emissions are highest along the

613 Russian coast, Svalbard, and in the Central Arctic, but they are much lower on the Arc-
614 tic scale. As a result, they contribute relatively little to emissions in the BOTH simu-
615 lation (Figure 6c), which are dominated by surface snow. We also show in Figures 6d-
616 f that predicted BrO concentrations do not directly correlate to the Br₂ emissions loca-
617 tions.

618 Figures 6g-i show that, in April 2012, the surface snow mechanism is the main driver
619 for large scale ozone depletion over most parts of the Arctic. This also shows that the
620 effect of blowing snow is much smaller during this month, contributing at most to 10 to
621 20 % of total depletion along Eastern Russia (supplementary Figure S7). We also note
622 that ozone depletion and BrO are not well correlated in the central Arctic, where BrO
623 formation is limited by near-total ozone depletion (mean concentrations ~5 ppbv, Fig-
624 ure S6). Ozone depletion also extends further inland into the Arctic than bromine ac-
625 tivation, as indicated by BrO concentrations.

626 In order to show the impact of this chemistry for oxidation in the Arctic bound-
627 ary layer, Figure 7a presents the OH/HO₂ ratio for the NOHALO run, which is in the
628 range of 0-0.03 for the Arctic and near 0 over most of the Arctic ocean. Figure 7b shows
629 the difference in this ratio upon including halogen chemistry in the model. The OH/HO₂
630 ratio increases by up to 0.03 over regions of the Arctic and Arctic Ocean upon includ-
631 ing halogen chemistry. This is equal to the largest OH/HO₂ ratio in the base run far from
632 the Arctic Ocean. This indicates that the boundary layer over the Arctic Ocean may have
633 oxidation conditions that are very different from most models at present, making it dif-
634 ficult to predict the lifetime of gas-phase organics and aerosol precursors emitted from
635 the Arctic Ocean during spring.

636 **6 Spring 2012 in the context of meteorological conditions and past stud-** 637 **ies**

638 Our results indicate that surface snow was the main driver of ozone depletion events
639 in the Arctic during Spring 2012. In agreement with previous work (Yang et al., 2019),
640 we show that blowing snow has a strong impact on Arctic sea salt aerosol concentrations
641 (supplementary Figure S1). However, in contradiction with previous work (Huang & Jaeglé,
642 2017; Huang et al., 2020; Yang et al., 2020), we find that blowing snow has little effect
643 on Arctic ozone depletion, being responsible only for a few events and, regionally, at most
644 for 10 to 20% of the total depletion in a limited region along the Russian Coast. Here
645 we explore some possible causes for these differences.

646 We think it is unlikely that our implementation underestimates blowing-snow sourced
647 Br₂ emissions, since we found that sea salt aerosol emissions from blowing snow are likely
648 overestimated in our implementation (supplementary Figure S1 and associated discus-
649 sion). We used a high value of 0.38 for the depletion factor, meaning that 38% of all avail-
650 able bromine from these overestimated blowing snow sea salt emissions is emitted in our
651 implementation. In addition, our study is to our knowledge the first to jointly assess model
652 performance for surface meteorology, sea salt, ground based BrO, and surface ozone in-
653 cluding central Arctic ozone, and none of these model/measurement comparisons indi-
654 cate model deficiencies which could explain these differences.

655 Falk and Sinnhuber (2018) indicate that the surface snow mechanism leads observa-
656 tions by up to 2 days at Alert, Canada. In order to examine if blowing snow is bet-
657 ter at reproducing the timing of the depletion events, rather than their magnitude, we
658 also perform a time-lagged correlation analysis (supplementary Figure S11). We do not
659 find the same leading time lag than Falk and Sinnhuber (2018) at any coastal site nor
660 at O-buoy 6, where the max correlation is reached at or very near a 0 h time-lag. We
661 remind that the (0 h lag) correlation is always higher in SURFACE than in BLOWING,
662 except for O-buoy6 where the highest correlation is found for NOHALO. Since BLOW-

ING has little effect on central Arctic ozone, it is closer to NOHALO and thus has a higher correlation than SURFACE at O-buoy6, even though it is strongly biased against observations. At O-buoy4, the correlation exhibits a maximum at -2 days for all simulations (SURFACE, NOHALO and BLOWING). Since this also occurs in NOHALO, this is most likely caused by a time lag in the meteorological reanalysis, and not to the implementation of the surface or blowing snow schemes. This is a known issue in the Arctic and especially in the central Arctic, where observations remain sparse and models, including reanalysis, have known problems reproducing meteorological systems.

We also examine if the lower role of blowing snow in ozone depletion found in our work could be due to meteorological differences in spring 2012 compared to other years. For example, in our simulations, wind speeds over Arctic sea ice, where salty blowing snow originates, are rarely above the critical threshold of 7 m/s (Supplementary Figure S4), and this threshold is exceeded even less often at the Arctic coastal sites (Supplementary Figure S5). We find (Supplementary Figure S9) that the blowing snow scheme emits sea salt aerosols as intended when this threshold is exceeded. Putting March-April 2012 into the long-term context, we find that wind speed was actually higher than normal over most of the Arctic (Supplementary Figure S8), which should in theory increase the influence of blowing snow in our simulations compared to earlier studies in other years. In addition, the Arctic surface was also mostly colder than average in March-April 2012 (Supplementary Figure S8), possibly indicating more stable conditions than usual, which could also intensify ODEs. Therefore, we conclude that it is unlikely that meteorological differences are to blame for the lower role of blowing snow in ozone depletion compared to earlier work.

In order to assess if 2012 was indeed a higher year in terms of bromine activity, we calculate the mean ozone concentration in March-April 2012 in Utqiagvik, and compare it to the long-term March-April mean for the 40 years 1973-2012. We also calculate the mean number of hours with depleted ozone (<10 ppbv) during the same March-April period. Excluding the 10 years with insufficient data quality (more than 10% of missing data), we find that March-April 2012 was particularly active, with the second lowest mean ozone concentration in that record (12.2 ppbv, compared to a long-term mean of 20.3 ppbv), and the largest number of hours of depleted ozone (817 h, compared to a long-term average of 425 h). We think this high prevalence of ODEs in this season confirms that this period is particularly suited for investigating the origin of these events.

7 Conclusions

In this work, we have implemented descriptions of halogen chemistry, activation and recycling within the WRF-Chem model. To our knowledge, this work is the first to implement both blowing snow and surface snow emissions of bromine into a single model, in order to compare their effects on springtime ozone depletion in the Arctic. We show that, in spring 2012, both bromine emission mechanisms can play a role in ozone depletion. Surface snow activation and recycling of bromine could be the key mechanism across most of the Arctic, while blowing snow could play an important role at specific sites and in initiating select events. We also show that the location of Br_2 emissions are not necessarily correlated with either BrO or ozone depletion. Further, we show that including this chemistry significantly increases the OH/HO_2 ratio at the surface regionally, especially over the Arctic Ocean.

Our results show, in agreement with previous studies, that blowing snow could be a strong source of sea salt aerosols over sea ice during spring. However, in contradiction with previous modeling work, we find that blowing snow has little effect on Arctic ozone depletion. We believe these differences can only be answered by completing a joint model study for the same time periods, using the same model input datasets (emissions, meteorology) and the same parameters, in order to compare the different components of

714 the ozone and bromine budgets in these models. We think such a study will be extremely
715 valuable to better understand the causes of Arctic ozone depletion, the sources of bromine,
716 and to further improve models. The heterogeneous (include super-cooled liquid and ice
717 phase) chemistry of sea salt aerosols during Arctic spring as well as snow pack chemistry
718 are both still uncertain despite existing studies (Oum et al., 1998; Huff & Abbatt, 2002;
719 Hunt et al., 2004; Pratt et al., 2013; Edebeli et al., 2020). Further experiments under
720 controlled lab conditions are needed to better understand bromine release from these sur-
721 faces in the future.

722 In the future, we also hope to investigate the relative roles of these processes in the
723 Antarctic, where wind speeds are higher and blowing snow could be more important, and
724 in other locations and years as new observations become available.

725 Our results provide a basis for future improvements in model predictions of sur-
726 face ozone at the regional scale by improving the representation of Arctic halogen chem-
727 istry and determining the activation pathways of reactive bromine within WRF-Chem.
728 In the future, we aim to test how these mechanisms operate under past and future sea
729 ice/snow cover conditions. Improved model predictions of polar halogen chemistry for
730 ODEs and bromine activation events will allow us to better understand the oxidative pro-
731 cesses for elemental mercury that lead to AMDEs and mercury deposition.

732 The functioning of atmospheric chemistry system in the lowest portion of the Arctic
733 atmosphere may fundamentally change as the Arctic warms and ice and snow cover
734 are reduced. Emissions from snow and ice will change as sea ice retreats, becomes thin-
735 ner, more saline, and as snow on sea ice changes. Chemistry within the Arctic bound-
736 ary layer determines the conditions that oceanic, ice, and snow emissions experience. Pro-
737 cesses in the lowest portion of the atmosphere are also important because this is where
738 species are most likely to be directly deposited back to the Arctic ocean, ice, and snow.
739 It is only by developing predictive models that include halogen chemistry that we will
740 be able to fully understand the influence of future environmental changes (including sea
741 ice change) and anthropogenic influences will have within the Arctic region.

742 **Acknowledgments**

743 This research has received funding from the European Union's Horizon 2020 research and
744 innovation program under grant agreement no. 689443 via project iCUPE (Integrative
745 and Comprehensive Understanding on Polar Environments). This work also supported
746 by the CNRS INSU LEFE-CHAT program under the grant Brom-Arc. We acknowledge
747 supported for M.F. from the Natural Environment Research Council (UK) grants NE/J023051/1
748 and NE/J020303/1. We acknowledge support for W.S. from the National Science Foun-
749 dation grant ARC-1602716. This work was performed using HPC resources from GENCI-
750 IDRIS (Grant A007017141) and the IPSL mesoscale computing center (CICLAD: Cal-
751 cul Intensif pour le CLimat, l'Atmosphère et la Dynamique). We thank the WRF-Chem
752 development and support teams at NOAA, NCAR, and PNNL for their support and col-
753 laborations. We acknowledge NCAR ACOM for providing the WRF-Chem chemical bound-
754 ary conditions used in this study. We acknowledge use of the WRF-Chem pre-processor
755 tools provided by the Atmospheric Chemistry Observations and Modeling Lab (ACOM)
756 of NCAR. We acknowledge the NOAA Global Monitoring Laboratory Earth System Re-
757 search Laboratories and the O-Buoy program for providing observations used in this study.
758 The BROMEX measurements are currently being archived at [https://asdc.larc.nasa](https://asdc.larc.nasa.gov)
759 [.gov](https://asdc.larc.nasa.gov) and currently available by contacting B. Simpson by email (wrsimpson@alaska.edu).
760 The O-buoy data is available from [https://arcticdata.io/catalog/view/doi%3A10](https://arcticdata.io/catalog/view/doi%3A10.18739%2FA2WD4W)
761 [.18739%2FA2WD4W](https://arcticdata.io/catalog/view/doi%3A10.18739%2FA2WD4W). We thank colleagues in France and internationally for helpful scien-
762 tific and technical discussions including: Jerome Fast, Louisa Emmons, John Orlando,
763 Jeroen Sonke, Kenjiro Toyota, Kerri Pratt, Paul Shepson, Jean-Christophe Raut, Didier
764 Voisin, Luke Surl, Tjarda Roberts, Kathy Law, Onishi Tatsuo, and Holger Sihler. The

code used for this study is available on Zenodo as Marelle et al. (2021) <https://doi.org/10.5281/zenodo.4607934>.

References

- Abbatt, J. P. D., Thomas, J. L., Abrahamsson, K., Boxe, C., Granfors, A., Jones, A. E., ... Yang, X. (2012). Halogen activation via interactions with environmental ice and snow in the polar lower troposphere and other regions. *Atmospheric Chemistry and Physics*, *12*(14), 6237–6271. doi: 10.5194/acp-12-6237-2012
- Aguzzi, A., & J. Rossi, M. (1999). The kinetics of the heterogeneous reaction of BrONO₂ with solid alkali halides at ambient temperature. A comparison with the interaction of ClONO₂ on NaCl and KBr. *Physical Chemistry Chemical Physics*, *1*, 4337–4346. Retrieved from <http://dx.doi.org/10.1039/A904611I> doi: 10.1039/A904611I
- Ammann, M., Cox, R. A., Crowley, J. N., Jenkin, M. E., Mellouki, A., Rossi, M. J., ... Wallington, T. J. (2013). Evaluated kinetic and photochemical data for atmospheric chemistry: Volume VI heterogeneous reactions with liquid substrates. *Atmospheric Chemistry and Physics*, *13*(16), 8045–8228. Retrieved from <https://acp.copernicus.org/articles/13/8045/2013/> doi: 10.5194/acp-13-8045-2013
- Anderson, P. S., & Neff, W. D. (2008). Boundary layer physics over snow and ice. *Atmospheric Chemistry and Physics*, *8*(13), 3563–3582. Retrieved from <https://acp.copernicus.org/articles/8/3563/2008/> doi: 10.5194/acp-8-3563-2008
- Atkinson, R., Baulch, D. L., Cox, R. A., Crowley, J. N., Hampson, R. F., Hynes, R. G., ... Wallington, T. J. (2008). Evaluated kinetic and photochemical data for atmospheric chemistry: Volume IV gas phase reactions of organic halogen species. *Atmospheric Chemistry and Physics*, *8*(15), 4141–4496. Retrieved from <https://www.atmos-chem-phys.net/8/4141/2008/> doi: 10.5194/acp-8-4141-2008
- Badia, A., Reeves, C. E., Baker, A. R., Saiz-Lopez, A., Volkamer, R., Koenig, T. K., ... von Glasow, R. (2019). Importance of reactive halogens in the tropical marine atmosphere: a regional modelling study using WRF-Chem. *Atmospheric Chemistry and Physics*, *19*(5), 3161–3189. Retrieved from <https://acp.copernicus.org/articles/19/3161/2019/> doi: 10.5194/acp-19-3161-2019
- Barrie, L. A. (1986). Arctic air pollution: An overview of current knowledge. *Atmospheric Environment*, *20*(4), 643 - 663. doi: [http://dx.doi.org/10.1016/0004-6981\(86\)90180-0](http://dx.doi.org/10.1016/0004-6981(86)90180-0)
- Barrie, L. A., Bottenheim, J. W., Schnell, R. C., Crutzen, P. J., & Rasmussen, R. A. (1988). Ozone destruction and photochemical reactions at polar sunrise in the lower Arctic atmosphere. *Nature*, *334*(6178), 138–141. doi: 10.1038/334138a0
- Berg, L. K., Shrivastava, M., Easter, R. C., Fast, J. D., Chapman, E. G., Liu, Y., & Ferrare, R. A. (2015). A new WRF-Chem treatment for studying regional-scale impacts of cloud processes on aerosol and trace gases in parameterized cumuli. *Geoscientific Model Development*, *8*(2), 409–429. Retrieved from <https://gmd.copernicus.org/articles/8/409/2015/> doi: 10.5194/gmd-8-409-2015
- Bleischmidt, A.-M., Richter, A., Burrows, J. P., Kaleschke, L., Strong, K., Theys, N., ... Zien, A. (2016). An exemplary case of a bromine explosion event linked to cyclone development in the Arctic. *Atmospheric Chemistry and Physics*, *16*(3), 1773–1788. Retrieved from <https://acp.copernicus.org/articles/16/1773/2016/> doi: 10.5194/acp-16-1773-2016
- Bougoudis, I., Bleischmidt, A.-M., Richter, A., Seo, S., Burrows, J. P., Theys, N.,

- 818 & Rinke, A. (2020). Long-term Time-series of Arctic Tropospheric BrO de-
 819 rived from UV-VIS Satellite Remote Sensing and its Relation to First Year
 820 Sea Ice. *Atmospheric Chemistry and Physics Discussions*, 2020, 1–38. Re-
 821 trieved from <https://acp.copernicus.org/preprints/acp-2020-116/> doi:
 822 10.5194/acp-2020-116
- 823 Brioude, J., Arnold, D., Stohl, A., Cassiani, M., Morton, D., Seibert, P., ...
 824 Wotawa, G. (2013). The Lagrangian particle dispersion model FLEXPART-
 825 WRF version 3.1. *Geoscientific Model Development*, 6(6), 1889–1904. doi:
 826 10.5194/gmd-6-1889-2013
- 827 Burd, J. A., Peterson, P. K., Nghiem, S. V., Perovich, D. K., & Simpson, W. R.
 828 (2017). Snowmelt onset hinders bromine monoxide heterogeneous recycling
 829 in the Arctic. *Journal of Geophysical Research: Atmospheres*, 122(15), 8297-
 830 8309. Retrieved from [https://agupubs.onlinelibrary.wiley.com/doi/abs/](https://agupubs.onlinelibrary.wiley.com/doi/abs/10.1002/2017JD026906)
 831 [10.1002/2017JD026906](https://agupubs.onlinelibrary.wiley.com/doi/abs/10.1002/2017JD026906) doi: 10.1002/2017JD026906
- 832 Burkholder, J., Sander, S., Abbatt, J., Barker, J., Huie, R., Kolb, C., ... Wine, P.
 833 (2015). *Chemical Kinetics and Photochemical Data for Use in Atmospheric*
 834 *Studies: Evaluation Number 18* (Tech. Rep.). Jet Propulsion Laboratory,
 835 Pasadena, CA. Retrieved from <http://jpldataeval.jpl.nasa.gov>
- 836 Carter, W. P. L. (2000). *Documentation of the SAPRC-99 chemical mechanism for*
 837 *VOC reactivity assessment. Final Report to California Air Resources Board*
 838 *Contract 92-329 and Contract 95-308*, (Tech. Rep.). Air Pollution Research
 839 Center and College of Engineering Center for Environmental Research and
 840 Technology, University of California Riverside.
- 841 Dee, D. P., Uppala, S. M., Simmons, A. J., Berrisford, P., Poli, P., Kobayashi,
 842 S., ... Vitart, F. (2011). The ERA-Interim reanalysis: configuration
 843 and performance of the data assimilation system. *Quarterly Journal*
 844 *of the Royal Meteorological Society*, 137(656), 553-597. Retrieved from
 845 <https://rmets.onlinelibrary.wiley.com/doi/abs/10.1002/qj.828> doi:
 846 10.1002/qj.828
- 847 Deiber, G., George, C., Le Calvé, S., Schweitzer, F., & Mirabel, P. (2004). Up-
 848 take study of ClONO₂ and BrONO₂ by Halide containing droplets. *At-*
 849 *mospheric Chemistry and Physics*, 4(5), 1291–1299. Retrieved from
 850 <https://acp.copernicus.org/articles/4/1291/2004/> doi: 10.5194/
 851 acp-4-1291-2004
- 852 Dentener, F. J., & Crutzen, P. J. (1993). Reaction of N₂O₅ on tropospheric
 853 aerosols: Impact on the global distributions of NO_x, O₃, and OH. *Journal*
 854 *of Geophysical Research: Atmospheres*, 98(D4), 7149-7163. Retrieved from
 855 <https://agupubs.onlinelibrary.wiley.com/doi/abs/10.1029/92JD02979>
 856 doi: 10.1029/92JD02979
- 857 Durre, I., Vose, R. S., & Wuertz, D. B. (2006). Overview of the Integrated Global
 858 Radiosonde Archive. *Journal of Climate*, 19(1), 53-68. Retrieved from
 859 <https://doi.org/10.1175/JCLI3594.1> doi: 10.1175/JCLI3594.1
- 860 Edebeli, J., Trachsel, J. C., Avak, S. E., Ammann, M., Schneebeli, M., Eichler, A.,
 861 & Bartels-Rausch, T. (2020). Snow heterogeneous reactivity of bromide
 862 with ozone lost during snow metamorphism. *Atmospheric Chemistry and*
 863 *Physics*, 20(21), 13443–13454. Retrieved from [https://acp.copernicus.org/](https://acp.copernicus.org/articles/20/13443/2020/)
 864 [articles/20/13443/2020/](https://acp.copernicus.org/articles/20/13443/2020/) doi: 10.5194/acp-20-13443-2020
- 865 Emmons, L. K., Arnold, S. R., Monks, S. A., Huijnen, V., Tilmes, S., Law, K. S.,
 866 ... Helmig, D. (2015). The POLARCAT Model Intercomparison Project
 867 (POLMIP): overview and evaluation with observations. *Atmospheric Chem-*
 868 *istry and Physics*, 15(12), 6721–6744. doi: 10.5194/acp-15-6721-2015
- 869 Emmons, L. K., Walters, S., Hess, P. G., Lamarque, J.-F., Pfister, G. G., Fillmore,
 870 D., ... Kloster, S. (2010). Description and evaluation of the Model for Ozone
 871 and Related chemical Tracers, version 4 (MOZART-4). *Geoscientific Model*
 872 *Development*, 3(1), 43–67. doi: 10.5194/gmd-3-43-2010

- 873 Falk, S., & Sinnhuber, B.-M. (2018). Polar boundary layer bromine explosion
874 and ozone depletion events in the chemistry-climate model EMAC v2.52:
875 Implementation and evaluation of AirSnow algorithm. *Geoscientific Model*
876 *Development*, 11(3), 1115-1131. doi: 10.5194/gmd-11-1115-2018
- 877 Fast, J. D., Gustafson, W. L., Easter, R. C., Zaveri, R. A., Barnard, J. C., Chap-
878 man, E. G., ... Peckham, S. E. (2006). Evolution of ozone, particulates, and
879 aerosol direct radiative forcing in the vicinity of Houston using a fully cou-
880 pled meteorology-chemistry-aerosol model. *Journal of Geophysical Research:*
881 *Atmospheres*, 111(D21). doi: 10.1029/2005JD006721
- 882 Fernandez, R. P., Carmona-Balea, A., Cuevas, C. A., Barrera, J. A., Kinnison,
883 D. E., Lamarque, J.-F., ... Saiz-Lopez, A. (2019). Modeling the Sources
884 and Chemistry of Polar Tropospheric Halogens (Cl, Br, and I) Using the
885 CAM-Chem Global Chemistry-Climate Model. *Journal of Advances in*
886 *Modeling Earth Systems*, 11(7), 2259-2289. Retrieved from [https://](https://agupubs.onlinelibrary.wiley.com/doi/abs/10.1029/2019MS001655)
887 agupubs.onlinelibrary.wiley.com/doi/abs/10.1029/2019MS001655 doi:
888 10.1029/2019MS001655
- 889 Frey, M., Norris, S., Brooks, I., Anderson, P., Nishimura, K., Yang, X., ... Wolff,
890 E. (2020). First direct observation of sea salt aerosol production from blowing
891 snow above sea ice. *Atmospheric Chemistry and Physics*, 20, 2549-2578. doi:
892 10.5194/acp-20-2549-2020
- 893 Frey, M. M., & Nomura, D. (2019). *Salinity profiles of snow on sea ice and sea ice in*
894 *the Arctic Ocean during winter 2015*. UK Polar Data Centre, Natural Environ-
895 ment Research Council, UK Research & Innovation. Retrieved from [https://](https://doi.org/10.5285/6ed9f4ea-6b89-4059-84e3-5c4118b68db9)
896 doi.org/10.5285/6ed9f4ea-6b89-4059-84e3-5c4118b68db9 doi: 10.5285/
897 6ed9f4ea-6b89-4059-84e3-5c4118b68db9
- 898 Fuchs, N. A., & Sutugin, A. G. (1971). HIGH-DISPERSED AEROSOLS. In
899 G. M. Hidy & J. R. Brock (Eds.), *Topics in current aerosol research (part 2)*.
900 New York: Pergamon. doi: [https://doi.org/10.1016/B978-0-08-016674-2.50006](https://doi.org/10.1016/B978-0-08-016674-2.50006-6)
901 -6
- 902 Gong, S. L., Barrie, L. A., & Blanchet, J.-P. (1997). Modeling sea-salt aerosols
903 in the atmosphere: 1. model development. *Journal of Geophysical Re-*
904 *search: Atmospheres*, 102(D3), 3805-3818. Retrieved from [https://](https://agupubs.onlinelibrary.wiley.com/doi/abs/10.1029/96JD02953)
905 agupubs.onlinelibrary.wiley.com/doi/abs/10.1029/96JD02953 doi:
906 <https://doi.org/10.1029/96JD02953>
- 907 Gratz, L. E., Ambrose, J. L., Jaffe, D. A., Shah, V., Jaegl, L., Stutz, J., ... Stell, M.
908 (2015). Oxidation of mercury by bromine in the subtropical Pacific free tropo-
909 sphere. *Geophysical Research Letters*, 42(23), 10494-10502. Retrieved
910 from [https://agupubs.onlinelibrary.wiley.com/doi/abs/10.1002/](https://agupubs.onlinelibrary.wiley.com/doi/abs/10.1002/2015GL066645)
911 [2015GL066645](https://agupubs.onlinelibrary.wiley.com/doi/abs/10.1002/2015GL066645) doi: 10.1002/2015GL066645
- 912 Grell, G. A., Peckham, S. E., Schmitz, R., McKeen, S. A., Frost, G., Skamarock,
913 W. C., & Eder, B. (2005). Fully coupled "online" chemistry within
914 the WRF model. *Atmospheric Environment*, 39(37), 6957-6975. doi:
915 <http://dx.doi.org/10.1016/j.atmosenv.2005.04.027>
- 916 Halfacre, J. W., Knepp, T. N., Shepson, P. B., Thompson, C. R., Pratt, K. A., Li,
917 B., ... Richter, A. (2014). Temporal and spatial characteristics of ozone de-
918 pletion events from measurements in the arctic. *Atmospheric Chemistry and*
919 *Physics*, 14(10), 4875-4894. Retrieved from [https://acp.copernicus.org/](https://acp.copernicus.org/articles/14/4875/2014/)
920 [articles/14/4875/2014/](https://acp.copernicus.org/articles/14/4875/2014/) doi: 10.5194/acp-14-4875-2014
- 921 Herrmann, M., Sihler, H., Frieß, U., Wagner, T., Platt, U., & Gutheil, E. (2021).
922 Time-dependent 3d simulations of tropospheric ozone depletion events in the
923 arctic spring using the weather research and forecasting model coupled with
924 chemistry (wrf-chem). *Atmospheric Chemistry and Physics*, 21(10), 7611-7638.
925 Retrieved from <https://acp.copernicus.org/articles/21/7611/2021/>
926 doi: 10.5194/acp-21-7611-2021
- 927 Hong, S.-Y., Noh, Y., & Dudhia, J. (2006). A New Vertical Diffusion Package with

- 928 an Explicit Treatment of Entrainment Processes. *Monthly Weather Review*,
 929 *134*(9), 2318-2341. Retrieved from <https://doi.org/10.1175/MWR3199.1>
 930 doi: 10.1175/MWR3199.1
- 931 Huang, J., & Jaeglé, L. (2017). Wintertime enhancements of sea salt aerosol
 932 in polar regions consistent with a sea ice source from blowing snow. *At-*
 933 *mospheric Chemistry and Physics*, *17*(5), 3699–3712. Retrieved from
 934 <https://acp.copernicus.org/articles/17/3699/2017/> doi: 10.5194/
 935 acp-17-3699-2017
- 936 Huang, J., Jaeglé, L., Chen, Q., Alexander, B., Sherwen, T., Evans, M. J., ... Choi,
 937 S. (2020). Evaluating the impact of blowing-snow sea salt aerosol on spring-
 938 time BrO and O₃ in the Arctic. *Atmospheric Chemistry and Physics*, *20*(12),
 939 7335–7358. Retrieved from [https://acp.copernicus.org/articles/20/](https://acp.copernicus.org/articles/20/7335/2020/)
 940 [7335/2020/](https://acp.copernicus.org/articles/20/7335/2020/) doi: 10.5194/acp-20-7335-2020
- 941 Huang, J., Jaeglé, L., & Shah, V. (2018). Using CALIOP to constrain blow-
 942 ing snow emissions of sea salt aerosols over Arctic and Antarctic sea ice.
 943 *Atmospheric Chemistry and Physics*, *18*(22), 16253–16269. Retrieved
 944 from <https://acp.copernicus.org/articles/18/16253/2018/> doi:
 945 10.5194/acp-18-16253-2018
- 946 Huff, A. K., & Abbatt, J. P. D. (2002). Kinetics and product yields in the heteroge-
 947 neous reactions of hobr with ice surfaces containing nabr and nacl. *The Jour-*
 948 *nal of Physical Chemistry A*, *106*(21), 5279-5287. Retrieved from [https://doi](https://doi.org/10.1021/jp014296m)
 949 [.org/10.1021/jp014296m](https://doi.org/10.1021/jp014296m) doi: 10.1021/jp014296m
- 950 Hunt, S. W., Roeselov, M., Wang, W., Wingen, L. M., Knipping, E. M., Tobias,
 951 D. J., ... Finlayson-Pitts, B. J. (2004). Formation of molecular bromine
 952 from the reaction of ozone with deliquesced nabr aerosol: evidence for interface
 953 chemistry. *The Journal of Physical Chemistry A*, *108*(52), 11559-11572. Re-
 954 trieved from <https://doi.org/10.1021/jp0467346> doi: 10.1021/jp0467346
- 955 Iacono, M. J., Delamere, J. S., Mlawer, E. J., Shephard, M. W., Clough, S. A.,
 956 & Collins, W. D. (2008). Radiative forcing by long-lived greenhouse
 957 gases: Calculations with the AER radiative transfer models. *Journal of*
 958 *Geophysical Research: Atmospheres*, *113*(D13). Retrieved from [https://](https://agupubs.onlinelibrary.wiley.com/doi/abs/10.1029/2008JD009944)
 959 agupubs.onlinelibrary.wiley.com/doi/abs/10.1029/2008JD009944 doi:
 960 10.1029/2008JD009944
- 961 International Union of Pure and Applied Chemistry. (2009). *IUPAC Task Group on*
 962 *Atmospheric Chemical Kinetic Data Evaluation*. Retrieved from [http://iupac](http://iupac.pole-ether.fr)
 963 [.pole-ether.fr](http://iupac.pole-ether.fr)
- 964 Janji, Z. I. (1994). The Step-Mountain Eta Coordinate Model: Further De-
 965 velopments of the Convection, Viscous Sublayer, and Turbulence Closure
 966 Schemes. *Monthly Weather Review*, *122*(5), 927-945. Retrieved from
 967 [https://doi.org/10.1175/1520-0493\(1994\)122<0927:TSMECM>2.0.CO;2](https://doi.org/10.1175/1520-0493(1994)122<0927:TSMECM>2.0.CO;2)
 968 doi: 10.1175/1520-0493(1994)122(0927:TSMECM)2.0.CO;2
- 969 Jones, A. E., Anderson, P. S., Begoin, M., Brough, N., Hutterli, M. A., Marshall,
 970 G. J., ... Wolff, E. W. (2009). BrO, blizzards, and drivers of polar tropo-
 971 spheric ozone depletion events. *Atmospheric Chemistry and Physics*, *9*(14),
 972 4639–4652. Retrieved from [https://acp.copernicus.org/articles/9/4639/](https://acp.copernicus.org/articles/9/4639/2009/)
 973 [2009/](https://acp.copernicus.org/articles/9/4639/2009/) doi: 10.5194/acp-9-4639-2009
- 974 Knepp, T. N., Bottenheim, J., Carlsen, M., Carlson, D., Donohoue, D., Friederich,
 975 G., ... Wyss, P. J. (2010). Development of an autonomous sea ice teth-
 976 ered buoy for the study of ocean-atmosphere-sea ice-snow pack interactions:
 977 the o-buoy. *Atmospheric Measurement Techniques*, *3*(1), 249–261. Re-
 978 trieved from <https://amt.copernicus.org/articles/3/249/2010/> doi:
 979 10.5194/amt-3-249-2010
- 980 Knipping, E. M., Lakin, M. J., Foster, K. L., Jungwirth, P., Tobias, D. J., Ger-
 981 ber, R. B., ... Finlayson-Pitts, B. J. (2000). Experiments and Simulations
 982 of Ion-Enhanced Interfacial Chemistry on Aqueous NaCl Aerosols. *Science*,

- 983 288(5464), 301–306. Retrieved from [https://science.sciencemag.org/
984 content/288/5464/301](https://science.sciencemag.org/content/288/5464/301) doi: 10.1126/science.288.5464.301
- 985 Laskin, A., Wang, H., Robertson, W. H., Cowin, J. P., Ezell, M. J., & Finlayson-
986 Pitts, B. J. (2006). A New Approach to Determining Gas-Particle Reaction
987 Probabilities and Application to the Heterogeneous Reaction of Deli-
988 quesced Sodium Chloride Particles with Gas-Phase Hydroxyl Radicals. *The
989 Journal of Physical Chemistry A*, 110(36), 10619–10627. Retrieved from
990 <https://doi.org/10.1021/jp063263+> doi: 10.1021/jp063263+
- 991 Liao, J., Huey, L. G., Tanner, D. J., Brough, N., Brooks, S., Dibb, J. E., ...
992 Gorham, K. (2011). Observations of hydroxyl and peroxy radicals and the im-
993 pact of BrO at Summit, Greenland in 2007 and 2008. *Atmospheric Chemistry
994 and Physics*, 11(16), 8577–8591. Retrieved from [https://acp.copernicus
995 .org/articles/11/8577/2011/](https://acp.copernicus.org/articles/11/8577/2011/) doi: 10.5194/acp-11-8577-2011
- 996 Marelle, L., Raut, J.-C., Law, K. S., Berg, L. K., Fast, J. D., Easter, R. C., ...
997 Thomas, J. L. (2017). Improvements to the WRF-Chem 3.5.1 model for
998 quasi-hemispheric simulations of aerosols and ozone in the Arctic. *Geoscientific
999 Model Development*, 10(10), 3661–3677. doi: 10.5194/gmd-10-3661-2017
- 1000 Marelle, L., Thomas, J. L., Ahmed, S., Tuite, K., Stutz, J., Dommergue, A.,
1001 ... Baladima, F. (2021). *WRF-Chem 4.1.1 version including polar
1002 bromine chemistry and emissions*. Zenodo. Retrieved 2021-03-16, from
1003 <https://zenodo.org/record/4607934> doi: 10.5281/zenodo.4607934
- 1004 Massom, R. A., Eicken, H., Hass, C., Jeffries, M. O., Drinkwater, M. R., Sturm, M.,
1005 ... Allison, I. (2001). Snow on Antarctic sea ice. *Reviews of Geophysics*,
1006 39(3), 413–445. Retrieved from [https://agupubs.onlinelibrary.wiley
1007 .com/doi/abs/10.1029/2000RG000085](https://agupubs.onlinelibrary.wiley.com/doi/abs/10.1029/2000RG000085) doi: 10.1029/2000RG000085
- 1008 Monks, S. A., Arnold, S. R., Emmons, L. K., Law, K. S., Turquety, S., Duncan,
1009 B. N., ... Ancellet, G. (2015). Multi-model study of chemical and phys-
1010 ical controls on transport of anthropogenic and biomass burning pollution
1011 to the Arctic. *Atmospheric Chemistry and Physics*, 15(6), 3575–3603. doi:
1012 10.5194/acp-15-3575-2015
- 1013 Morrison, H., Thompson, G., & Tatarskii, V. (2009). Impact of Cloud Microphysics
1014 on the Development of Trailing Stratiform Precipitation in a Simulated Squall
1015 Line: Comparison of One- and Two-Moment Schemes. *Monthly Weather
1016 Review*, 137(3), 991–1007. Retrieved from [https://doi.org/10.1175/
1017 2008MWR2556.1](https://doi.org/10.1175/2008MWR2556.1) doi: 10.1175/2008MWR2556.1
- 1018 Nakanishi, M., & Niino, H. (2009). Development of an Improved Turbulence Closure
1019 Model for the Atmospheric Boundary Layer. *Journal of the Meteorological So-
1020 ciety of Japan*, 87(5), 895–912. doi: 10.2151/jmsj.87.895
- 1021 National Centers for Environmental Prediction. (2000). *NCEP FNL Operational
1022 Model Global Tropospheric Analyses, continuing from July 1999*. Boulder
1023 CO: Research Data Archive at the National Center for Atmospheric Re-
1024 search, Computational and Information Systems Laboratory. Retrieved from
1025 <https://doi.org/10.5065/D6M043C6>
- 1026 Niu, G.-Y., Yang, Z.-L., Mitchell, K. E., Chen, F., Ek, M. B., Barlage, M., ... Xia,
1027 Y. (2011). The community Noah land surface model with multiparameteriza-
1028 tion options (Noah-MP): 1. Model description and evaluation with local-scale
1029 measurements. *Journal of Geophysical Research: Atmospheres*, 116(D12).
1030 Retrieved from [https://agupubs.onlinelibrary.wiley.com/doi/abs/
1031 10.1029/2010JD015139](https://agupubs.onlinelibrary.wiley.com/doi/abs/10.1029/2010JD015139) doi: 10.1029/2010JD015139
- 1032 Oleson, K. W., Lawrence, D. M., Bonan, G. B., Flanner, M. G., Kluzek, E.,
1033 Lawrence, P. J., ... Decker, M. (2010). *Technical Description of version
1034 4.0 of the Community Land Model (CLM)*.
- 1035 Oltmans, S. J. (1981). Surface ozone measurements in clean air. *Journal of Geophys-
1036 ical Research: Oceans*, 86(C2), 1174–1180. doi: 10.1029/JC086iC02p01174
- 1037 Oum, K. W., Lakin, M. J., & Finlayson-Pitts, B. J. (1998). Bromine activa-

- 1038 tion in the troposphere by the dark reaction of O_3 with seawater ice. *Geo-*
 1039 *physical Research Letters*, 25(21), 3923–3926. Retrieved from [https://](https://agupubs.onlinelibrary.wiley.com/doi/abs/10.1029/1998GL900078)
 1040 agupubs.onlinelibrary.wiley.com/doi/abs/10.1029/1998GL900078 doi:
 1041 <https://doi.org/10.1029/1998GL900078>
- 1042 Peterson, P. K., Hartwig, M., May, N. W., Schwartz, E., Rigor, I., Ermold, W.,
 1043 ... Pratt, K. A. (2019). Snowpack measurements suggest role for multi-
 1044 year sea ice regions in Arctic atmospheric bromine and chlorine chem-
 1045 istry. *Elementa Science of the Anthropocene*, 7(14). Retrieved from
 1046 <http://doi.org/10.1525/elementa.352> doi: 10.1525/elementa.352
- 1047 Peterson, P. K., Pöhler, D., Sihler, H., Zielcke, J., General, S., Frie, U., ... Pratt,
 1048 K. A. (2017). Observations of bromine monoxide transport in the Arctic
 1049 sustained on aerosol particles. *Atmospheric Chemistry and Physics*, 17(12),
 1050 7567–7579. Retrieved from [https://acp.copernicus.org/articles/17/](https://acp.copernicus.org/articles/17/7567/2017/)
 1051 [7567/2017/](https://acp.copernicus.org/articles/17/7567/2017/) doi: 10.5194/acp-17-7567-2017
- 1052 Peterson, P. K., Simpson, W. R., Pratt, K. A., Shepson, P. B., Frieß, U., Zielcke, J.,
 1053 ... Nghiem, S. V. (2015). Dependence of the vertical distribution of bromine
 1054 monoxide in the lower troposphere on meteorological factors such as wind
 1055 speed and stability. *Atmospheric Chemistry and Physics*, 15(4), 2119–2137.
 1056 Retrieved from <https://acp.copernicus.org/articles/15/2119/2015/>
 1057 [doi: 10.5194/acp-15-2119-2015](https://acp.copernicus.org/articles/15/2119/2015/)
- 1058 Piot, M., & Glasow, R. v. (2009). Modelling the multiphase near-surface chemistry
 1059 related to ozone depletions in polar spring. *Journal of Atmospheric Chemistry*,
 1060 64(2), 77–105. Retrieved from [https://doi.org/10.1007/s10874-010-9170-](https://doi.org/10.1007/s10874-010-9170-1)
 1061 [-1](https://doi.org/10.1007/s10874-010-9170-1) doi: 10.1007/s10874-010-9170-1
- 1062 Platt, U., & Hönninger, G. (2003). The role of halogen species in the troposphere.
 1063 *Chemosphere*, 52(2), 325 - 338. doi: [https://doi.org/10.1016/S0045-6535\(03\)](https://doi.org/10.1016/S0045-6535(03)00216-9)
 1064 [00216-9](https://doi.org/10.1016/S0045-6535(03)00216-9)
- 1065 Pratt, K. A., Custard, K. D., Shepson, P. B., Douglas, T. A., Phler, D., General, S.,
 1066 ... Stirm, B. H. (2013). Photochemical production of molecular bromine in
 1067 Arctic surface snowpacks. *Nature Geoscience*, 6(5), 351–356. Retrieved from
 1068 <https://doi.org/10.1038/ngeo1779> doi: 10.1038/ngeo1779
- 1069 Pratte, P., & Rossi, M. J. (2006). The heterogeneous kinetics of HOBr and HOCl
 1070 on acidified sea salt and model aerosol at 4090% relative humidity and ambient
 1071 temperature. *Physical Chemistry Chemical Physics*, 8, 3988–4001. Retrieved
 1072 from <http://dx.doi.org/10.1039/B604321F> doi: 10.1039/B604321F
- 1073 Provost, C., Sennchael, N., Miguet, J., Itkin, P., Rsel, A., Koenig, Z., ... Granskog,
 1074 M. A. (2017). Observations of flooding and snow-ice formation in a thinner
 1075 arctic sea-ice regime during the n-ice2015 campaign: Influence of basal ice
 1076 melt and storms. *Journal of Geophysical Research: Oceans*, 122(9), 7115–
 1077 7134. Retrieved from [https://agupubs.onlinelibrary.wiley.com/doi/abs/](https://agupubs.onlinelibrary.wiley.com/doi/abs/10.1002/2016JC012011)
 1078 [10.1002/2016JC012011](https://agupubs.onlinelibrary.wiley.com/doi/abs/10.1002/2016JC012011) doi: 10.1002/2016JC012011
- 1079 Rhodes, R. H., Yang, X., Wolff, E. W., McConnell, J. R., & Frey, M. M. (2017).
 1080 Sea ice as a source of sea salt aerosol to Greenland ice cores: a model-based
 1081 study. *Atmospheric Chemistry and Physics*, 17(15), 9417–9433. Retrieved
 1082 from <https://acp.copernicus.org/articles/17/9417/2017/> doi:
 1083 [10.5194/acp-17-9417-2017](https://acp.copernicus.org/articles/17/9417/2017/)
- 1084 Sander, R. (2015). Compilation of Henry's law constants (version 4.0) for water as
 1085 solvent. *Atmospheric Chemistry and Physics*, 15(8), 4399–4981. Retrieved
 1086 from <https://www.atmos-chem-phys.net/15/4399/2015/> doi: 10.5194/acp-
 1087 [-15-4399-2015](https://www.atmos-chem-phys.net/15/4399/2015/)
- 1088 Sander, R., Keene, W. C., Pszenny, A. A. P., Arimoto, R., Ayers, G. P., Baboukas,
 1089 E., ... Van Dingenen, R. (2003). Inorganic bromine in the marine boundary
 1090 layer: a critical review. *Atmospheric Chemistry and Physics*, 3(5), 1301–1336.
 1091 Retrieved from <https://acp.copernicus.org/articles/3/1301/2003/> doi:
 1092 [10.5194/acp-3-1301-2003](https://acp.copernicus.org/articles/3/1301/2003/)

- 1093 Seinfeld, J. H., & Pandis, S. N. (1998). *Atmospheric Chemistry and Physics: From*
 1094 *air pollution to climate change*. New York: John Wiley & Sons.
- 1095 Seisel, S., Flckiger, B., & Rossi, M. J. (1998). The heterogeneous reaction of
 1096 N_2O_5 with HBr on Ice comparison with N_2O_5+HCl . *Berichte der Bun-*
 1097 *sengesellschaft fr physikalische Chemie*, 102(6), 811-820. Retrieved from
 1098 <https://onlinelibrary.wiley.com/doi/abs/10.1002/bbpc.19981020604>
 1099 doi: 10.1002/bbpc.19981020604
- 1100 Simpson, W. R., Brown, S. S., Saiz-Lopez, A., Thornton, J. A., & von Glasow, R.
 1101 (2015). Tropospheric Halogen Chemistry: Sources, Cycling, and Impacts.
 1102 *Chemical Reviews*, 115(10), 4035–4062. doi: 10.1021/cr5006638
- 1103 Simpson, W. R., Carlson, D., Hönninger, G., Douglas, T. A., Sturm, M., Per-
 1104 ovich, D., & Platt, U. (2007a). First-year sea-ice contact predicts bromine
 1105 monoxide (BrO) levels at Barrow, Alaska better than potential frost
 1106 flower contact. *Atmospheric Chemistry and Physics*, 7(3), 621–627. Re-
 1107 trieved from <https://acp.copernicus.org/articles/7/621/2007/> doi:
 1108 10.5194/acp-7-621-2007
- 1109 Simpson, W. R., Perovich, D., Matrai, P., Shepson, P., & Chavez, F. (2009). *The*
 1110 *Collaborative O-Buoy Project: Deployment of a Network of Arctic Ocean*
 1111 *Chemical Sensors for the IPY and beyond*. Arctic Data Center. Retrieved from
 1112 <https://arcticdata.io/catalog/view/doi%3A10.18739%2FA2WD4W> doi:
 1113 10.18739/A2WD4W
- 1114 Simpson, W. R., Peterson, P., Frieß, U., Sihler, H., Lampel, J., Platt, U., ...
 1115 Nghiem, S. (2017). Horizontal and vertical structure of reactive bromine
 1116 events probed by bromine monoxide MAX-DOAS. *Atmospheric Chemistry and*
 1117 *Physics*, 17(15), 9291–9309. doi: 10.5194/acp-17-9291-2017
- 1118 Simpson, W. R., von Glasow, R., Riedel, K., Anderson, P., Ariya, P., Bottenheim,
 1119 J., ... Wolff, E. (2007b). Halogens and their role in polar boundary-layer
 1120 ozone depletion. *Atmospheric Chemistry and Physics*, 7(16), 4375–4418. doi:
 1121 10.5194/acp-7-4375-2007
- 1122 Spolaor, A., Vallelonga, P., Plane, J. M. C., Kehrwald, N., Gabrieli, J., Varin, C.,
 1123 ... Barbante, C. (2013). Halogen species record Antarctic sea ice extent over
 1124 glacialinterglacial periods. *Atmospheric Chemistry and Physics*, 13(13), 6623–
 1125 6635. Retrieved from [https://acp.copernicus.org/articles/13/6623/](https://acp.copernicus.org/articles/13/6623/2013/)
 1126 2013/ doi: 10.5194/acp-13-6623-2013
- 1127 Spolaor, A., Vallelonga, P., Turetta, C., Maffezzoli, N., Cozzi, G., Gabrieli, J., ...
 1128 Dahl-Jensen, D. (2016). Canadian Arctic sea ice reconstructed from bromine
 1129 in the Greenland NEEM ice core. *Scientific Reports*, 6(1), 33925. Retrieved
 1130 from <https://doi.org/10.1038/srep33925> doi: 10.1038/srep33925
- 1131 Sterk, H. A. M., Steeneveld, G. J., Vihma, T., Anderson, P. S., Bosveld, F. C., &
 1132 Holtslag, A. A. M. (2015). Clear-sky stable boundary layers with low winds
 1133 over snow-covered surfaces. part 1: Wrf model evaluation. *Quarterly Jour-*
 1134 *nal of the Royal Meteorological Society*, 141(691), 2165-2184. Retrieved from
 1135 <https://rmets.onlinelibrary.wiley.com/doi/abs/10.1002/qj.2513> doi:
 1136 <https://doi.org/10.1002/qj.2513>
- 1137 Stohl, A., Forster, C., Frank, A., Seibert, P., & Wotawa, G. (2005). Tech-
 1138 nical note: The Lagrangian particle dispersion model FLEXPART ver-
 1139 sion 6.2. *Atmospheric Chemistry and Physics*, 5(9), 2461–2474. doi:
 1140 10.5194/acp-5-2461-2005
- 1141 Stutz, J., Thomas, J. L., Hurlock, S. C., Schneider, M., von Glasow, R., Piot, M., ...
 1142 Lefer, B. L. (2011). Longpath DOAS observations of surface BrO at Summit,
 1143 Greenland. *Atmospheric Chemistry and Physics*, 11(18), 9899–9910. Re-
 1144 trieved from <https://acp.copernicus.org/articles/11/9899/2011/> doi:
 1145 10.5194/acp-11-9899-2011
- 1146 Swanson, W. F., Graham, K. A., Halfacre, J. W., Holmes, C. D., Shepson, P. B.,
 1147 & Simpson, W. R. (2020). Arctic Reactive Bromine Events Occur in Two

- 1148 Distinct Sets of Environmental Conditions: A Statistical Analysis of 6 Years
 1149 of Observations. *Journal of Geophysical Research: Atmospheres*, 125(10),
 1150 e2019JD032139. Retrieved from [https://agupubs.onlinelibrary.wiley](https://agupubs.onlinelibrary.wiley.com/doi/abs/10.1029/2019JD032139)
 1151 [.com/doi/abs/10.1029/2019JD032139](https://agupubs.onlinelibrary.wiley.com/doi/abs/10.1029/2019JD032139) doi: 10.1029/2019JD032139
- 1152 Tewari, M., Chen, F., Wang, W., Dudhia, J., LeMone, M. A., Gayno, G., ...
 1153 Cuenca, R. H. (2004). Implementation and verification of the unified Noah
 1154 land surface model in the WRF model. In *20th Conference on Weather Anal-*
 1155 *ysis and Forecasting/16th Conference on Numerical Weather Prediction* (pp.
 1156 11–15).
- 1157 Thomas, J. L., Dibb, J. E., Huey, L. G., Liao, J., Tanner, D., Lefer, B., ... Stutz,
 1158 J. (2012a). Modeling chemistry in and above snow at Summit, Greenland
 1159 Part 2: Impact of snowpack chemistry on the oxidation capacity of the bound-
 1160 ary layer. *Atmospheric Chemistry and Physics*, 12(14), 6537–6554. Re-
 1161 trieved from <https://acp.copernicus.org/articles/12/6537/2012/> doi:
 1162 10.5194/acp-12-6537-2012
- 1163 Thomas, J. L., Dibb, J. E., Stutz, J., von Glasow, R., Brooks, S., Huey, L. G., &
 1164 Lefer, B. (2012b). Overview of the 2007 and 2008 campaigns conducted as
 1165 part of the Greenland Summit Halogen-HOx Experiment (GSHOX). *Atmo-*
 1166 *spheric Chemistry and Physics*, 12(22), 10833–10839.
- 1167 Thomas, J. L., Stutz, J., Lefer, B., Huey, L. G., Toyota, K., Dibb, J. E., & von
 1168 Glasow, R. (2011). Modeling chemistry in and above snow at Summit, Green-
 1169 land Part 1: Model description and results. *Atmospheric Chemistry and*
 1170 *Physics*, 11(10), 4899–4914. Retrieved from [https://acp.copernicus.org/](https://acp.copernicus.org/articles/11/4899/2011/)
 1171 [articles/11/4899/2011/](https://acp.copernicus.org/articles/11/4899/2011/) doi: 10.5194/acp-11-4899-2011
- 1172 Toyota, K., McConnell, J., Lupu, A., Neary, L., Mclinden, C., Richter, A., ... Sioris,
 1173 C. (2011). Analysis of reactive bromine production and ozone depletion in
 1174 the Arctic boundary layer using 3-D simulations with GEM-AQ: Inference
 1175 from synoptic-scale patterns. *Atmospheric Chemistry and Physics*, 11(8),
 1176 3949–3979. doi: 10.5194/acp-11-3949-2011
- 1177 Toyota, K., McConnell, J. C., Staebler, R. M., & Dastoor, A. P. (2014). Airsnow-
 1178 pack exchange of bromine, ozone and mercury in the springtime Arctic simu-
 1179 lated by the 1-D model PHANTAS - Part 1: In-snow bromine activation and
 1180 its impact on ozone. *Atmospheric Chemistry and Physics*, 14(8), 4101–4133.
 1181 Retrieved from <https://acp.copernicus.org/articles/14/4101/2014/>
 1182 doi: 10.5194/acp-14-4101-2014
- 1183 von Glasow, R., Sander, R., Bott, A., & Crutzen, P. J. (2002a). Modeling halogen
 1184 chemistry in the marine boundary layer 1. Cloud-free MBL. *Journal of Geo-*
 1185 *physical Research: Atmospheres*, 107(D17). Retrieved from [https://agupubs](https://agupubs.onlinelibrary.wiley.com/doi/abs/10.1029/2001JD000942)
 1186 [.onlinelibrary.wiley.com/doi/abs/10.1029/2001JD000942](https://agupubs.onlinelibrary.wiley.com/doi/abs/10.1029/2001JD000942) doi: 10.1029/
 1187 2001JD000942
- 1188 von Glasow, R., Sander, R., Bott, A., & Crutzen, P. J. (2002b). Modeling halogen
 1189 chemistry in the marine boundary layer 2. Interactions with sulfur and the
 1190 cloud-covered MBL. *Journal of Geophysical Research: Atmospheres*, 107(D17).
 1191 Retrieved from [https://agupubs.onlinelibrary.wiley.com/doi/abs/](https://agupubs.onlinelibrary.wiley.com/doi/abs/10.1029/2001JD000943)
 1192 [10.1029/2001JD000943](https://agupubs.onlinelibrary.wiley.com/doi/abs/10.1029/2001JD000943) doi: 10.1029/2001JD000943
- 1193 Wang, C., Graham, R. M., Wang, K., Gerland, S., & Granskog, M. A. (2019).
 1194 Comparison of era5 and era-interim near-surface air temperature, snow-
 1195 fall and precipitation over arctic sea ice: effects on sea ice thermodynam-
 1196 ics and evolution. *The Cryosphere*, 13(6), 1661–1679. Retrieved from
 1197 <https://tc.copernicus.org/articles/13/1661/2019/> doi: 10.5194/
 1198 tc-13-1661-2019
- 1199 Wang, S., McNamara, S. M., Moore, C. W., Obrist, D., Steffen, A., Shepson, P. B.,
 1200 ... Pratt, K. A. (2019). Direct detection of atmospheric atomic bromine lead-
 1201 ing to mercury and ozone depletion. *Proceedings of the National Academy of*
 1202 *Sciences*, 116(29), 14479–14484. doi: 10.1073/pnas.1900613116

- 1203 Wesely, M. (1989). Parameterization of surface resistances to gaseous dry depo-
1204 sition in regional-scale numerical models. *Atmospheric Environment*, *23*(6),
1205 1293–1304. doi: [http://dx.doi.org/10.1016/0004-6981\(89\)90153-4](http://dx.doi.org/10.1016/0004-6981(89)90153-4)
- 1206 Wild, O., Zhu, X., & Prather, M. J. (2000). Fast-J: Accurate Simulation of In- and
1207 Below-Cloud Photolysis in Tropospheric Chemical Models. *Journal of Atmo-*
1208 *spheric Chemistry*, *37*(3), 245–282. doi: 10.1023/A:1006415919030
- 1209 Yang, X., Blechschmidt, A.-M., Bognar, K., McClure-Begley, A., Morris, S.,
1210 Petropavlovskikh, I., ... Zhao, X. (2020). Pan-Arctic surface ozone: modelling
1211 vs measurements. *Atmospheric Chemistry and Physics Discussions*, *2020*, 1–
1212 33. Retrieved from <https://acp.copernicus.org/preprints/acp-2019-984/>
1213 doi: 10.5194/acp-2019-984
- 1214 Yang, X., Frey, M. M., Rhodes, R. H., Norris, S. J., Brooks, I. M., Anderson, P. S.,
1215 ... Wolff, E. W. (2019). Sea salt aerosol production via sublimating wind-
1216 blown saline snow particles over sea ice: parameterizations and relevant micro-
1217 physical mechanisms. *Atmospheric Chemistry and Physics*, *19*(13), 8407–8424.
1218 Retrieved from <https://acp.copernicus.org/articles/19/8407/2019/>
1219 doi: 10.5194/acp-19-8407-2019
- 1220 Yang, X., Pyle, J. A., & Cox, R. A. (2008). Sea salt aerosol production and bromine
1221 release: Role of snow on sea ice. *Geophysical Research Letters*, *35*(16). doi: 10
1222 .1029/2008GL034536
- 1223 Yang, X., Pyle, J. A., Cox, R. A., Theys, N., & Van Roozendaal, M. (2010).
1224 Snow-sourced bromine and its implications for polar tropospheric ozone.
1225 *Atmospheric Chemistry and Physics*, *10*(16), 7763–7773. Retrieved
1226 from <https://acp.copernicus.org/articles/10/7763/2010/> doi:
1227 10.5194/acp-10-7763-2010
- 1228 Zaveri, R. A., Easter, R. C., Fast, J. D., & Peters, L. K. (2008). Model for Simu-
1229 lating Aerosol Interactions and Chemistry (MOSAIC). *Journal of Geophysical*
1230 *Research: Atmospheres*, *113*(D13). doi: 10.1029/2007JD008782

Accepted Article

Figure 1. Simulation domain, sea ice at the beginning of the simulation, location of the measurement sites, and 60 degrees north latitude circle.

Figure 2. (a) 2-meter temperature observed (black) and simulated by our selected WRF setup (blue) at Utqiagvik, Alaska. (b) Average temperature profile observed by radiosondes over Utqiagvik (black) during the same period, and interpolated (land points only) at the same locations and times in our selected WRF setup (blue).

Figure 3. (Top) O_3 observed (black) at Utqiagvik, Alaska and simulated by WRF-Chem in the NOHALO (blue), SURFACE (orange), BLOWING (yellow) and BOTH (purple) simulations. (Middle) BrO observed by MAX-DOAS during the BROMEX campaign at Utqiagvik, and simulated by WRF-Chem. (Bottom) Br_2 simulated by WRF-Chem at Utqiagvik.

Figure 4. Surface ozone observed (black) and simulated by WRF-Chem (color) at (a) Station Nord, Greenland; (b) Tiksi, Russia; (c) Summit, Greenland; (d) Zeppelin Station, Svalbard; (e) O-buoy4, central Arctic; (f) O-buoy6, central Arctic

Figure 5. FLEXPART-WRF 7-day backward potential emission sensitivity (PES) (a) 0-100 m PES for releases when measured O_3 was below 10 ppbv and (b) 0-5000 m PES for when O_3 exceeded 30 ppbv. Monthly average fractional sea ice coverage, as represented in WRF, for April 2012 is shaded in grey. (c) The altitude (above sea level) of the air mass trajectories, up to 7 days prior to the release, for high background ozone (blue) and low background ozone (red), with RMS error bars.

Accepted Article

Figure 6. Monthly averaged (1 to 30 April 2012) changes in modeled quantities in each simulation, compared to NOHALO. Modeled Br₂ emissions (top), BrO concentrations (middle) and surface ozone concentrations (bottom). Changes predicted across the Arctic for SURFACE-NOHALO (left panels), BLOWING-NOHALO (center panels), and BOTH-NOHALO (right panels).

Accepted Article

Figure 7. (a) OH/HO₂ ratio in the NOHALO run (b) increase in the OH/HO₂ ratio upon including halogen chemistry, given as the difference between the BOTH and NOHALO runs: $(\text{OH}/\text{HO}_2)_{\text{BOTH}} - (\text{OH}/\text{HO}_2)_{\text{NOHALO}}$.

Table 1. Root Mean Square Error (RMSE) and correlation coefficient (R) between WRF simulations and temperature observations (IGRA radiosondes, surface measurements from NOAA) at Utqiagvik, Alaska. Selected model setup for this study is shown in bold.

Driving model	Surface	Boudary layer	R_{IGRA}	$RMSE_{IGRA}$ (K)	$R_{surface}$	$RMSE_{surface}$ (K)
ERA-Interim	CLM	YSU	0.44	2.21	0.94	4.34
ERA-Interim	CLM	MYNN2	0.48	2.59	0.94	4.37
ERA-Interim	Noah-MP	YSU	0.47	2.27	0.94	4.00
ERA-Interim	Noah-MP	MYJ	0.49	2.55	0.94	4.23
ERA-Interim	Noah-MP	MYNN2	0.48	2.55	0.94	4.09
ERA-Interim	Noah LSM	YSU	0.49	2.57	0.94	3.94
ERA-Interim	Noah LSM	MYJ	0.49	2.16	0.95	3.84
ERA-Interim	Noah LSM	MYNN2	0.46	2.60	0.95	3.92
FNL	CLM	YSU	0.46	2.23	0.93	4.13
FNL	CLM	MYNN2	0.45	2.60	0.93	4.20
FNL	Noah LSM	YSU	0.47	2.23	0.94	3.77
FNL	Noah LSM	MYJ	0.51	2.58	0.94	3.76
FNL	Noah LSM	MYNN2	0.53	2.53	0.94	3.79

Table 2. Heterogeneous reactions, reaction probabilities (γ) and yields (ϕ).

Reaction	Representation in WRF-Chem	γ and ϕ	Ref.
$\text{HOCl} \xrightarrow{\text{aerosol}} \text{Cl}_2$	$\text{HOCl}(\text{+HCl}) \rightarrow \text{Cl}_2$	$\gamma = 0.0004, \phi = 0.5$	a
$\text{HOCl} \xrightarrow{\text{aerosol}} \text{BrCl}$	$\text{HOCl}(\text{+HBr}) \rightarrow \text{BrCl}$	$\gamma = 0.0004, \phi = 0.5$	a
$\text{ClONO}_2 \xrightarrow{\text{aerosol}} \text{Cl}_2 + \text{HNO}_3$	$\text{ClONO}_2(\text{+HCl}) \rightarrow \text{Cl}_2 + \text{HNO}_3$	$\gamma = 0.11, \phi = 0.27$	b
$\text{ClONO}_2 \xrightarrow{\text{aerosol}} \text{BrCl} + \text{HNO}_3$	$\text{ClONO}_2(\text{+HBr}) \rightarrow \text{BrCl} + \text{HNO}_3$	$\gamma = 0.11, \phi = 0.46$	b
$\text{ClONO}_2 \xrightarrow{\text{aerosol}} \text{HOCl} + \text{HNO}_3$	$\text{ClONO}_2 \rightarrow \text{HOCl} + \text{HNO}_3$	$\gamma = 0.11, \phi = 0.27$	b
$\text{HOBr} \xrightarrow{\text{aerosol}} \text{Br}_2$	$\text{HOBr}(\text{+HBr}) \rightarrow \text{Br}_2$	$\gamma = 0.1, \phi = 0.5$	c,d
$\text{HOBr} \xrightarrow{\text{aerosol}} \text{BrCl}$	$\text{HOBr}(\text{+HCl}) \rightarrow \text{BrCl}$	$\gamma = 0.1, \phi = 0.5$	c,d
$\text{BrONO}_2 \xrightarrow{\text{aerosol}} \text{Br}_2$	$\text{BrONO}_2(\text{+HBr}) \rightarrow \text{Br}_2$	$\gamma = 0.14, \phi = 0.42$	e
$\text{BrONO}_2 \xrightarrow{\text{aerosol}} \text{BrCl}$	$\text{BrONO}_2(\text{+HCl}) \rightarrow \text{BrCl}$	$\gamma = 0.14, \phi = 0.29$	e
$\text{BrONO}_2 \xrightarrow{\text{aerosol}} \text{HOBr} + \text{HNO}_3$	$\text{BrONO}_2 \rightarrow \text{HOBr} + \text{HNO}_3$	$\gamma = 0.14, \phi = 0.29$	e
$\text{N}_2\text{O}_5 \xrightarrow{\text{aerosol}} \text{BrNO}_2 + \text{HNO}_3$	$\text{N}_2\text{O}_5(\text{+HBr}) \rightarrow \text{BrNO}_2 + \text{HNO}_3$	$\gamma = 0.044, \phi = 0.24$	f
$\text{OH} \xrightarrow{\text{aerosol}} \text{Cl}_2$	$\text{OH}(\text{+HCl}) \rightarrow 0.5*\text{Cl}_2$	$\gamma = 0.2, \phi = 0.5$	g,h

^aAmmann et al. (2013)^cPratte and Rossi (2006)^eDeiber et al. (2004)^gKnipping et al. (2000)^bAguzzi and J. Rossi (1999)^dInternational Union of Pure and Applied Chemistry (2009)^fSeisel et al. (1998)^hLaskin et al. (2006)

Table 3. Parameters for the dry deposition scheme: Henry’s law constant (H^*), Henry’s law temperature correction factor (DHR), deposition reactivity parameter (f_0), molecular diffusivity (dv_j).

Species	H^* ($\text{mol m}^{-3} \text{ hPa}^{-1}$)	DHR (K)	f_0	dv_j ($\text{cm}^{-2} \text{ s}^{-1}$)
Br_2	0.730	4400	1	0.079
HOBr	6000	0	1	0.102
HBr	24.3	370	0	0.111
BrONO_2	24.3	370	1	0.084
Cl_2	0.0932	2000	1	0.12
HOCl	659	5900	1	0.14
ClONO_2	1510	2300	1	0.1

Table 4. Description of the simulations performed in this study.

Simulation name	Description
NOHALO	No halogen chemistry and no updates included
SURFACE	Only surface activation mechanism implemented (as described by Toyota et al. (2011))
BLOWING	Only blowing snow parameterization included (as proposed by Yang et al. (2008) using param
BOTH	Both SURFACE and BLOWING mechanisms operating



